IEEE ComSoc IEEE Open Journal of the Communications Society

An Affine Precoded Superimposed Pilot Based mmWave MIMO-OFDM ISAC System

AWADHESH GUPTA [1] (Student Member, IEEE), MEESAM JAFRI [1] (Student Member, IEEE), SURAJ SRIVASTAVA [2] (Member, IEEE), ADITYA K. JAGANNATHAM [1] (Senior Member, IEEE), AND LAJOS HANZO [2] (Life Fellow, IEEE)

[1]Department of Electrical Engineering, Indian Institute of Technology Kanpur, Kanpur 208016, India
[2]Department of Electrical Engineering, Indian Institute of Technology Jodhpur, Jodhpur, Rajasthan 342030, India
[3]School of Electronics and Computer Science, University of Southampton, Southampton SO17 1BJ, U.K.

CORRESPONDING AUTHOR: L. HANZO (e-mail: lh@ecs.soton.ac.uk).

The work of Aditya K. Jagannatham was supported in part by the Qualcomm Innovation Fellowship, and in part by the Arun Kumar Chair Professorship.
L. Hanzo would like to acknowledge the financial support of the Engineering and Physical Sciences Research Council projects EP/W016605/1, EP/X01228X/1, and EP/Y026721/1 as well as of the European Research Council's Advanced Fellow Grant QuantCom (Grant No. 789028).

ABSTRACT A new affine-precoded superimposed pilot (AP-SIP) scheme is conceived for both wireless channel and radar target parameter estimation in a millimeter wave (mmWave) multiple-input multiple-output (MIMO) orthogonal frequency division multiplexing (OFDM)-based integrated sensing and communication (ISAC) systems. The AP-SIP scheme leads to enhanced estimation accuracy and improved utilization of spectral resources. Initially, the pilot-assisted radar (PAR) and data-assisted radar (DAR) parameter estimation models are separately developed for the estimation of the radar target parameters. Subsequently, these are combined into a joint pilot-data radar (JPDR) model for simultaneously harnessing both the signals to further boost the estimation accuracy. The sparse Bayesian learning (BL)-based joint-BL (J-BL) technique is developed for this system that efficiently exploits the sparsity of the radar scattering environment. Next, a group sparse BL (G-BL) technique is also derived that exploits the group sparsity across subcarriers for the estimation of the wireless beamspace channel vector, which outperforms the competing techniques, including conventional sparse BL. The optimal pilot, transmit precoder (TPC) and receive combiner (RC) are determined at the dual-function radar-communication (DFRC) base station (BS) and also at the user equipment (UE) for maximizing the performance attained. The Bayesian Cramer-Rao bounds (BCRB) are explicitly derived to benchmark the performance of the wireless channel and radar target parameter estimation. Simulation results are provided to demonstrate the improved performance of the proposed schemes considering multiple metrics, such as the normalized mean squared error (NMSE), bit error rate (BER) and achievable spectral efficiency (ASE).

INDEX TERMS Integrated sensing and communication (ISAC), dual-function radar-communication (DFRC), millimeter wave (mmWave), affine-precoded superimposed-pilot (AP-SIP), Bayesian Learning (BL).

I. INTRODUCTION

THE exponential increase in the number of wireless devices and the demand for high data rates has led to a significant congestion in the existing spectral bands [1]–[3]. A cutting edge innovation to address this challenge is to exploit the abundant spectrum in the millimeter wave (mmWave) band for future wireless communication networks [4], [5]. Nevertheless, a notable segment of the frequency spectrum in these bands is currently designated for radar systems, emphasizing the need to integrate sensing and communication functionalities into a unified platform to meet the desired throughput targets. This has led to a substantial interest in the adoption of integrated sensing and communication (ISAC) systems, which facilitate the simultaneous operation of both systems via the deployment of a dual-function radar-communication (DFRC) transceiver [6], [7].

TABLE 1: LIST OF ACRONYMS

AoA	Angle of Arrival
AoD	Angle of Departure
AP-SIP	Affine-Precoded Superimposed Pilot
APES	Angle and Phase Estimation
BL	Bayesian Learning
BS	Base Station
BCRB	Bayesian Cramér-Rao Bound
BFIM	Bayesian Fisher Information Matrix
CSI	Channel State Information
CFR	Channel Frequency Response
DFRC	Dual-Function Radar-Communication
DAR	Data-Assisted Radar
DoF	Degrees-of-Freedom
DA-BL	Data-Assisted Bayesian Learning
FD	Frequency-Domain
FOCUSS	Focal Underdetermined System Solver
G-BL	Group BL
HAD	Hybrid Analog-Digital
ISAC	Integrated Sensing and Communication
JPDR	Joint Pilot-Data Radar
J-BL	Joint Bayesian Learning
MIMO	Multiple-Input-Multiple-Output
MUI	Multi-User Interference
mmWave	Millimeter Wave
OFDM	Orthogonal Frequency Division Multiplexing
OMP	Orthogonal Matching Pursuit
PAR	Pilot-Assisted Radar
PA-BL	Pilot-Assisted Bayesian Learning
RAs	Receive Antennas
RC	Receive Combiner
RCS	Radar Cross-Section
RF	Radio Frequency
SNR	Signal-to-Noise Ratio
SIP	Superimposed pilot
TPC	Transmit Precoder
TAs	Transmit Antennas
TD	Time-Domain
UE	User-Equipment
ULA	Uniform Linear Array
UPA	Uniform Planar Array

TABLE 2: LIST OF NOTATIONS

N_T	Number of transmit antennas at the DFRC BS
N_R	Number of receive antennas at the DFRC BS
N_{RF}	Number of RF chains at the DFRC BS
L_t	Number of targets/ scatterers
M_R	Number of receive antennas at the UE
M_{RF}	Number of RF chains at the UE
P	Number of angular bins at UE
Q	Number of angular bins at BS
R	Number of range bins
K	Number of Subcarriers
L	Number of OFDM blocks transmitted in a frame
N_F	Number of frames transmitted
M_P	Number of pilot beams transmitted in N_F frames
N_{CF}	Number of combining frames at the BS
N_C	Number of combining vectors at the BS
M_{CF}	Number of combining frames at the UE
M_{CU}	Number of combining vectors at the BS
α_t	Time-domain RCS coefficient of the target
β_l	Complex path gain of the lth scatterer
ϕ_l	AoA at the UE from the lth scatterer
θ_l	AoD/AoA at the DFRC BS from the lth target/scatterer
$\mathbf{a}_R$	Receive array response vector at the BS
$\mathbf{a}_T$	Transmit array response vector at the BS
$\mathbf{b}_R$	Array response vector at the UE
$\boldsymbol{\gamma}_t$	Time-domain RCS vector
$\mathbf{h}_f[k]$	CFR vector corresponding to kth subcarrier
$\mathbf{h}_{b,f}$	Joint beamspace channel vector
$\boldsymbol{\Gamma}_t$	Time-domain RCS matrix
$\mathbf{A}_R$	Receive codebook at BS
$\mathbf{A}_T$	Transmit codebook at BS
$\mathbf{B}_R$	Receive codebook at UE
$\mathbf{F}_{\text{RF}}$	Frequency-flat RF TPC at the BS
$\mathbf{W}_{\text{RF}}$	Frequency-flat RF RC at the BS
$\mathbf{W}_{\text{BB}}$	Frequency-selective baseband RC at the BS
$\mathbf{U}_{\text{RF}}$	Frequency-flat RF RC at the UE
$\mathbf{U}_{\text{BB}}$	Frequency-selective baseband RC at the UE
$\mathbf{H}_f[k]$	CFR matrix corresponding to the kth subcarrier
$\mathbf{H}_{b,f}[k]$	Beamspace CFR matrix corresponding to the kth subcarrier

Apart from the availability of much wider bandwidth, the short wavelength of mmWave frequencies allows one to pack large antenna arrays into devices having compact form factors that can enable highly directional beamforming. Thus, multiple-input-multiple-output (MIMO) technology can be exploited to obtain high beamforming gains for mitigating the effects of path loss, atmospheric absorption and penetration losses that can otherwise cause a significant hindrance to communication in the mmWave band [8], [9]. Furthermore, the deployment of a large number of antennas at the DFRC transceiver can also lead to a significant improvement in radar performance due to simultaneous transmission/reception of multiple probing signals. This results in a remarkable increase in the number of degrees-of-freedom (DoF), in turn leading to a substantial improvement in the estimation accuracy [10]. However, it is difficult to implement such a DFRC MIMO transceiver in the high-frequency mmWave band as the conventional fully digital architecture requires a single radio frequency (RF) chain for each antenna element. This poses a significant obstacle at mmWave frequencies since assigning a dedicated RF chain for each antenna element results in significantly higher power consumption coupled with soaring costs and complexity. To overcome this impediment and pave the way for the

practical realization of mmWave MIMO DFRC transceivers, one can exploit the path-breaking hybrid signal processing architecture that mandates a substantially reduced number of RF chains than the traditional fully-digital architecture [11], [12]. Orthogonal frequency division multiplexing (OFDM) is eminently suitable for mmWave MIMO DFRC systems due to its resilience to both multipath and inter-symbol-interference (ISI) effects as well as owing to its potential of achieving excellent performance in radar systems [13]. The orthogonality of the OFDM waveform guaranteed by the discrete Fourier transform (DFT) and inverse DFT (IDFT) operations at the receiver and transmitter, respectively, can facilitate signal processing for both communications and radar sensing. However, the availability of accurate channel state information (CSI) plays a pivotal role in the design of hybrid transmit precoders (TPC) and receive combiners (RC), especially in wideband ISAC systems that transmit over multiple subcarriers. Existing approaches for CSI and radar parameter estimation in mmWave MIMO-OFDM ISAC systems usually employ time-multiplexed pilot and data signals to avoid mutual interference between them [14]. However, this time-multiplexing is highly inefficient, since the pilot signals do not convey any information. In such techniques, the pilot signal requires additional spectral resources that could otherwise be used for data transmission. To enhance the spectral efficiency, sophisticated methods were introduced in [15], where the training signal is directly superimposed onto the data signals. Nonetheless, this results in interference between the data and training sequences, ultimately resulting in a reduction of the estimation accuracy. The affine-precoded superimposed pilot (AP-SIP) framework is a novel technique that linearly precodes the pilot and data signals, thus allowing their simultaneous transmission. This naturally leads to a notable improvement in the spectral efficiency since both the pilot and data are transmitted in the same time-frequency slot [16]. However, it is important to note that this does not affect the estimation and data decoding performance, because the data and pilot can be decoupled. A brief overview of existing contributions in related research is presented next.

A. State-of-the-art

In the recent literature on ISAC, OFDM is a popular waveform candidate for integrated sensing and communication [17]–[20]. Sturm *et al.* [17] explore the suitability of integrated sensing as well as communication and studied multiple DFRC waveforms for the estimation of the ranges as well as velocities of multiple radar targets and transmission of information symbols to a communication user. Shi *et al.* [18] proposed a joint subcarrier selection and power allocation scheme for minimizing the power consumption in an OFDM-ISAC system for communication-centric waveform design. The authors of [19] considered a radar-centric OFDM-based ISAC system and designed a radar waveform by optimizing the Fisher information and CRB, subject to both the interference caused to the communication system and to sub-carrier power ratio constraints. As a further development, the authors of [20] proposed a low peak-to-average power ratio (PAPR) waveform for OFDM-based DFRC and optimized a weighted objective function of multi-user interference (MUI) and of the ideal radar beampattern under power and PAPR constraints. The authors of [21] explored the trade-off between the detection probability and the achievable data rate in an ISAC system. Specifically, a power allocation problem is formulated in their work to minimize the transmit power at the DFRC BS, while maintaining the required detection probability for monitoring the target and meeting the achievable rate requirement of the communication user.

Note that all the treatises reviewed above consider the sub-6 GHz band for ISAC. Hence, they do not exploit the large blocks of spectrum offered by the mmWave bands. The authors of [22] described a novel inter-carrier interference (ICI) aware two-stage algorithm designed for target detection and parameter estimation. In their work, the MUltiple SIgnal Classification (MUSIC) algorithm was employed for estimating the target angles and subsequently, for each estimated angle, the delay and Doppler parameters were estimated via the popular angle and phase estimation (APES) approach. The authors of [23] developed a mmWave automotive radar model based on the IEEE 802.11ad standard to enable joint mmWave vehicular communication and radar operations in the 60 GHz band. Along similar lines, the authors of [24] studied the applicability of phase-modulated-continuous-wave (PMCW) and orthogonal-frequency-division-multiple-access (OFDMA) waveforms for a bistatic mmWave ISAC system. However, mmWave signals suffer from high propagation losses, increased signal blockage, and traditionally require a high number of power-hungry analog-to-digital converters (ADCs), digital-to-analog converters (DACs), and power amplifiers, which prohibit the assignment of individual RF chain for each antenna. This has motivated researchers to explore a hybrid analog-digital (HAD) beamforming structure for addressing these challenges.

In this context, Liu *et al.* [25] considered a hybrid beamforming architecture for an ISAC system and invoked conventional techniques such as the MUSIC algorithm, matched-filtering (MF) and APES for the estimation of the radar target and wireless channel parameters. However, this work considered the number of targets to be known at the DFRC BS, which is not feasible in practice. The authors of [26] proposed a transmit beamformer design scheme that effectively mitigates the interference between multiple users while simultaneously providing multiple beams for ISAC. The authors of [27] considered the beam-split effect encountered in the mmWave/Terahertz (THz) band and proposed a beam-split aware (BSA) algorithm. The BSA approach aims to enhancing the angle-of-arrival (AoA) and channel estimation performance by exploiting the angular deviations in the spatial domain caused by beam-split, followed by

utilizing the MUSIC algorithm for target parameter estimation. Liyanaarachchi *et al.* [28] proposed an IDFT based radar range profile estimation technique and subsequently, these range profiles are exploited for MUSIC-based AoA estimation. However, a key shortcoming of the various solutions reviewed above is that they fail to exploit the inherent sparsity of the scattering environment at mmWave frequencies, arising from the presence of only a few non-zero radar targets/ scatterers. Incorporating the sparsity may potentially lead to a remarkable improvement in the accuracy of target detection, radar parameter and channel estimation. Toward this, Rahman *et al.* [29] proposed a fast marginalized block sparse Bayesian learning (BL) algorithm (BSBL-FM) based one-dimension (1-D) target parameter estimation for multi-user MIMO-OFDMA systems. In their approach, the delay is initially estimated using the BSBL-FM algorithm. Subsequently, the rest of the sensing parameters are estimated by employing the amplitude estimates corresponding to the delays. Although these low-dimensional compressive sensing (CS) techniques have a significantly lower complexity, their estimation performance is modest [29]. As a further development, the authors of [30], in their pioneering work, proposed target parameter estimation relying on 1D, 2D and 3D CS target parameter estimation algorithms. The authors of [31] propose a novel orthogonal matching pursuit associated with a support refinement (OMP-SR) algorithm for radar sensing and channel estimation. Note that the existing schemes designed for sparse parameter estimation in mmWave MIMO-OFDM ISAC systems typically use time-multiplexed pilot and data signals to avoid mutual interference. The pilot sequence in such schemes occupies a large fraction of the limited bandwidth, which results in substantially reduced spectral efficiency. Very few studies have been conducted in the literature to leverage the superimposed pilot (SIP)-based framework for radar target parameter and channel estimation in a ISAC system. In this regard, Bao *et al.* [32] proposed an SIP framework for a bistatic ISAC system in the sub-6 GHz band. In the scheme proposed therein, the channel is initially estimated using only the pilot signal. The data symbols are decoded in the next step using the channel estimate obtained previously, followed by target parameter estimation using both pilot and data symbols. However, the systems of [32] do not incorporate the HAD transceiver architecture, which is crucial for the realization of communication and sensing in the mmWave band. Moreover, the inherent sparsity is not capitalized on for target parameter/ channel estimation.

To overcome these shortcomings in the existing literature, we develop and analyze sparse estimation algorithms designed for target sensing and channel state information (CSI) acquisition in mmWave MIMO-OFDM ISAC systems, relying on the affine-precoded SIP (AP-SIP) framework. This leads to a notable improvement in the spectral efficiency because the pilot and data are transmitted in the same time-frequency slot in a superimposed fashion, while simultaneously allowing us to estimate the target parameters and communication channel. Table I contrasts the contributions of this paper to those in the existing literature discussed above. Next, we provide a brief overview of the various contributions of this paper.

B. Contributions

1) This paper considers a mmWave MIMO-OFDM ISAC system relying on hybrid signal processing architecture and presents the design and analysis of an affine-precoded superimposed pilot (AP-SIP) signal for sparse radar target parameter and wireless channel estimation, followed by data detection at the user equipment (UE). It is worth noting that affine-precoded superimposed pilot (AP-SIP) signaling in sub-6 GHz can not be directly extended in the mmWave band. In sub-6 GHz MIMO systems, the presence of a rich scattering environment and a fully digital architecture allows for transmitting a single block of SIP symbols, effectively facilitating radar/ channel parameter estimation. On the contrary, the mmWave MIMO systems pose challenges for estimation due to their hybrid analog-digital precoding architecture and the limited number of angularly sparse multipath components. Unlike sub-6 GHz systems, the prevalent mmWave MIMO target parameter/ channel estimation schemes require multiple reconfigurations of the analog precoder's phases during the estimation process to excite all angular modes of the mmWave MIMO channel. To address this, an intelligent framewise signal processing is proposed.
2) Initially, a linear model is derived for sparse radar target parameter estimation that exploits the bandwidth-efficient AP-SIP signal. Subsequently, pure pilot-assisted Bayesian learning (PA-BL) and data-assisted BL (DA-BL) algorithms are proposed for sparse radar parameter estimation at the DFRC BS. Next, the joint BL (J-BL) technique is derived together with the input-output model that exploits both pilot and data symbols for sparse estimation to achieve the best possible estimation accuracy.
3) Unlike conventional sparse recovery techniques, in which a sparsity constraint is imposed on individual elements, in this work, the signal is divided into multiple groups that can either simultaneously become zero or non-zero. A sparsity constraint is imposed on these groups, and this additional structural information can significantly enhance the quality of sparse signal recovery. Considering this, a group-sparse BL (G-BL) technique is derived for channel estimation, which exploits the group sparsity of the beamspace channel across subcarriers, and results in an improved performance in comparison to sparse Bayesian learning (SBL) and other conventional techniques, such as the FOcal Underdetermined System Solver (FOCUSS) [33] and orthogonal matching pursuit (OMP) [34].

TABLE 3: Contrasting our contributions to the literature

Features	[17]	[23]	[24]	[25]	[26]	[27]	[28]	[29]	[31]	[32]	Proposed
MIMO	✓	✓	✓	✓	✓	✓	✓	✓	✓	✓	✓
mmWave band		✓	✓	✓	✓	✓	✓		✓		✓
Hybrid architecture				✓	✓	✓	✓		✓		✓
Sparse model						C		✓	S		✓
Simultaneous sparsity								✓			✓
Bayesian Learning								✓			✓
SIP framework										✓	✓
Joint pilot-data radar model											✓
CRB			✓						✓		✓
Imaging	✓	✓	✓	✓			✓	✓	✓	✓	✓
Total coherence-based TPC, RC and pilot design											✓

Note C: only for communication channel estimation, S: only for sensing.

4) In sparse estimation problem $\mathbf{y} = \mathbf{\Phi x}$, The total coherence of the dictionary matrix $\mathbf{\Phi}$ can be defined as

$$\boldsymbol{\mu}^t(\mathbf{\Phi}) = \sum_m \sum_{m \neq n} \left| \mathbf{\Phi}(:,m)^H \mathbf{\Phi}(:,n) \right|^2 .$$

The recovery performance can be significantly improved by minimizing the total coherence of the dictionary matrix, which serves as an indicator of the correlation between the columns in a dictionary matrix $\mathbf{\Phi}$. The sparse signal can be accurately recovered using fewer measurements when the coherence is low [8], [35]. Therefore, the TPC, RC and pilot signals are designed by minimizing the total coherence of the dictionary matrices.

5) The Bayesian Cramér-Rao bounds (BCRBs) are derived for the estimates of the radar cross-section (RCS) coefficients of the targets and wireless channel in the ISAC system.
6) Exhaustive simulation results are presented for radar target parameter estimation, two-dimensional (2D) imaging, wireless channel estimation, data detection and the achievable spectral efficiency (ASE) to characterize the performance of the schemes proposed for mmWave MIMO-OFDM ISAC systems.

C. Organization of the paper

The rest of this paper is organized as follows. Section II introduces both the radar and communication system models. Section III presents the PA-BL, DA-BL and J-BL schemes followed by G-BL based wireless channel estimation in Section IV. Section V describes the design of the optimal TPC/ RC and pilot signals for the proposed systems. The BCRBs for the target parameter and wireless channel estimation are presented in Section VI. Extensive simulation results are presented in Section VII for characterising the performance and validating the analytical results. Section VIII concludes the paper.

Notations: The following notation is used throughout this paper. Vectors are denoted by boldface lower case letters while matrices are specified by boldface uppercase letters. The quantity $\mathrm{Diag}(\mathbf{a})$ denotes a diagonal matrix with elements of vector $\mathbf{a}$ as its principal diagonal, while $\mathrm{diag}(\mathbf{B})$ denotes the vector formed from the diagonal elements of a matrix $\mathbf{B}$. The quantity $\mathrm{blkdiag}\left(\mathbf{B}_1, \mathbf{B}_2, .., \mathbf{B}_N\right)$ represents a block-diagonal matrix comprising matrices $\mathbf{B}_1, \mathbf{B}_2, .., \mathbf{B}_N$ along the principal diagonal. The symbols $\odot$ and $\otimes$ denote the Khatri-Rao and Kronecker products, respectively. The symbols $*$ and $\circledast$ symbolize linear and circular convolution between two signals, respectively. The symbols $(\cdot)^T, (\cdot)^H, (\cdot)^*, (\cdot)^\dagger$ and $\mathrm{Tr}(\cdot)$ denote the transpose, Hermitian, conjugate, Moore-Penrose pseudoinverse, and trace of a matrix, respectively. The l_2, l_0 and Frobenius norms are denoted by $||\cdot||_2$, $||\cdot||_0$ and $||\cdot||_F$, respectively. The quantity $\mathrm{vec}(\cdot)$ represents the vector obtained by stacking the columns of the matrix and $\mathrm{vec}^{-1}(\cdot)$ reshapes a vector into a matrix. $\mathbb{E}\{\cdot\}$ denotes the expectation operator. The following property of a diagonal matrix $\mathbf{B}$ is also exploited in this paper for simplification $\mathrm{vec}(\mathbf{ABC}) = (\mathbf{C}^T \odot \mathbf{A})\mathrm{diag}(\mathbf{B})$.

II. Radar and Communication System models

Consider a colocated mmWave MIMO-OFDM ISAC system, wherein the DFRC BS is equipped with N_T transmit antennas (TAs), N_R receive antennas (RAs) and N_{RF} RF chains satisfying $N_{RF} \ll \min(N_T, N_R)$. The DFRC BS transmits $N_s < N_{RF}$ data streams to serve a user equipment (UE) having M_R RAs and M_{RF} RFCs, while simultaneously estimating the radar parameters of L_t targets that are at unknown locations in the environment, as shown in Fig. 1. The system under consideration operates in the full-duplex mode and, akin to several significant studies such as [25] and [29], self-interference cancellation is assumed at the DFRC receiver.

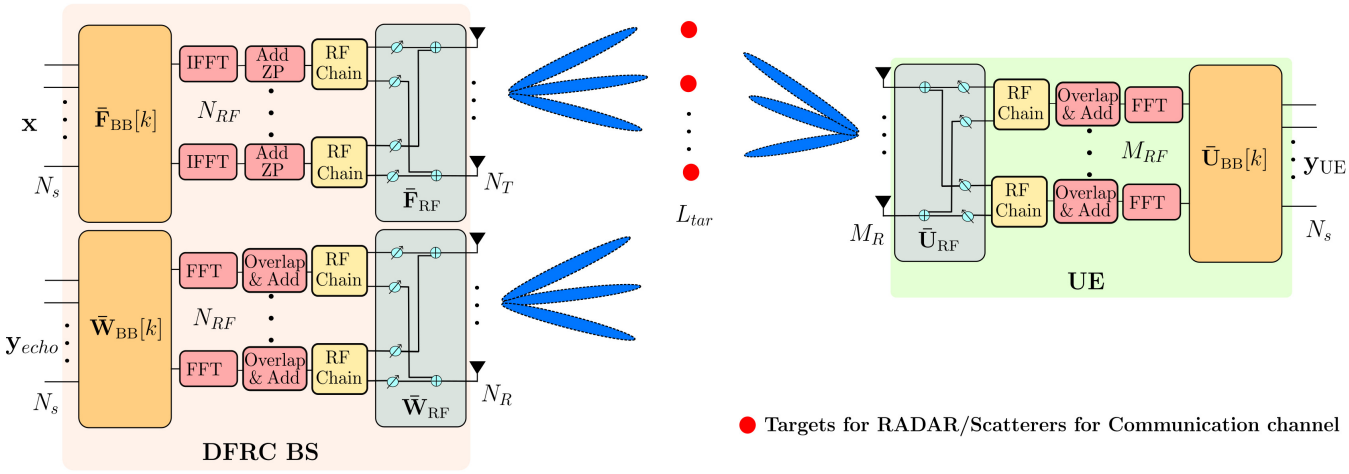

FIGURE 1: mmWave MIMO-OFDM Joint RadCom schematic for subcarrier k

A. Radar model

Consider the radar scattering environment to be partitioned into Q angle and R range bins. The L_t stationary targets are assumed to be randomly scattered at unknown locations. Let $\alpha_t(q,r)$ represent the time-domain RCS coefficient of the target present in the (q,r)th bin associated with a general target located at an angle θ_q and range R_r from the DFRC BS. The transmitted signal is reflected by a target located at a range R_r and received at the DFRC BS after a round trip delay of $\tau_r = 2R_r/c$, where c is the speed of light. Let $\mathbf{x}(n) \in \mathbb{C}^{N_{RF}\times 1}$ denote the signal vector transmitted by the DFRC BS at time instant n. The echo $\mathbf{y}_{\text{echo}}(n) \in \mathbb{C}^{N_S\times 1}$ received at the DFRC BS after combining can be expressed as

$$\mathbf{y}_{\text{echo}}(n) = \sum_{q=0}^{Q-1} \bar{\mathbf{W}}^H \mathbf{a}_R(\theta_q)\mathbf{a}_T^H(\theta_q)\bar{\mathbf{F}}_{\text{RF}}\mathbf{x}(n) * \alpha_t(q,n) + \bar{\mathbf{W}}^H\mathbf{v}(n), \tag{1}$$

where $\mathbf{v}(n)$ denotes the symmetric complex additive white Gaussian noise (AWGN) vector with distribution $\mathcal{CN}(0,\sigma_v^2\mathbf{I}_{N_R})$. Furthermore, $\bar{\mathbf{W}} = \bar{\mathbf{W}}_{\text{RF}}\bar{\mathbf{W}}_{\text{BB}} \in \mathbb{C}^{N_R\times N_S}$ denotes the hybrid RC at the DFRC BS, whereas the matrix $\bar{\mathbf{W}}_{\text{BB}} \in \mathbb{C}^{N_{RF}\times N_S}$ is the baseband RC. The matrices $\bar{\mathbf{W}}_{\text{RF}} \in \mathbb{C}^{N_R\times N_{RF}}$ and $\bar{\mathbf{F}}_{\text{RF}} \in \mathbb{C}^{N_T\times N_{RF}}$ represent the RF RC and RF TPC, respectively. The RF TPC and RC consist of a digitally controlled phase-shifter network. Hence, $\bar{\mathbf{W}}_{\text{RF}}$ and $\bar{\mathbf{F}}_{\text{RF}}$ must have constant-magnitude entries, which, without loss of generality can be set as $\left|\bar{\mathbf{W}}_{\text{RF}}(i,j)\right| = \frac{1}{\sqrt{N_R}}$ and $\left|\bar{\mathbf{F}}_{\text{RF}}(i,j)\right| = \frac{1}{\sqrt{N_T}}$ $\forall i,j$. The choice of zero-padding (ZP) is preferred instead of the cyclic prefix (CP) in mmWave MIMO OFDM systems, since it provides a time window for reconfiguration of the analog circuitry. The quantities $\mathbf{a}_R \in \mathbb{C}^{N_R\times 1}$ and $\mathbf{a}_T \in \mathbb{C}^{N_T\times 1}$ represent the receive and transmit array response vectors, which are given by

$$\mathbf{a}_T(\theta) = \left[1, e^{-j\frac{2\pi}{\lambda}d_T\sin(\theta)}, \ldots, e^{-j(N_T-1)\frac{2\pi}{\lambda}d_T\sin(\theta)}\right]^T, \tag{2}$$

$$\mathbf{a}_R(\theta) = \left[1, e^{-j\frac{2\pi}{\lambda}d_R\sin(\theta)}, \ldots, e^{-j(N_R-1)\frac{2\pi}{\lambda}d_R\sin(\theta)}\right]^T. \tag{3}$$

It is important to note that a uniform linear arrays (ULA) is assumed for both the system and for the channel models for simplicity. However, our approach can be readily extended to a uniform planar array (UPA).

B. Communication model

Assume that the multiple targets present in the scattering environment also act as potential scatterers for the communication channel. The received signal $\mathbf{y}_{\text{UE}} \in \mathbb{C}^{N_s\times 1}$ after combining at the UE can be expressed as

$$\mathbf{y}_{\text{UE}}[k] = \bar{\mathbf{U}}^H[k]\mathbf{H}_f[k]\bar{\mathbf{F}}_{\text{RF}}\mathbf{x}[k] + \bar{\mathbf{U}}^H[k]\mathbf{z}[k], \tag{4}$$

where $\bar{\mathbf{U}}[k] = \bar{\mathbf{U}}_{\text{RF}}\bar{\mathbf{U}}_{\text{BB}}[k] \in \mathbb{C}^{M_R\times N_s}$. The quantities $\bar{\mathbf{U}}_{\text{BB}}[k] \in \mathbb{C}^{M_{RF}\times N_s}$ and $\bar{\mathbf{U}}_{\text{RF}} \in \mathbb{C}^{M_R\times M_{RF}}$ denote the frequency selective-baseband RC and frequency flat RF RC, respectively. The RF RC is also constrained to constant magnitude elements, i.e., $\left|\bar{\mathbf{U}}_{\text{RF}}(i,j)\right| = \frac{1}{\sqrt{M_R}}$. The vector $\mathbf{z}[k]$ denotes the AWGN having the distribution $\mathcal{CN}(0,\sigma_z^2)$. Furthermore, $\mathbf{H}_f[k] \in \mathbb{C}^{M_R\times N_T}$ represents the channel frequency response (CFR) matrix corresponding to the kth subcarrier, which is formulated as [36]

$$\mathbf{H}_f(k) = \sum_{l=1}^{L_t} \beta_l e^{-j2\pi k\Delta f\tau_l}\mathbf{b}_R(\phi_l)\mathbf{a}_T^H(\theta_l), \tag{5}$$

where β_l is the complex path-gain and generated as independent and identically (i.i.d.) samples obeying the distribution $\mathcal{CN}(0,1)$. The quantities $\tau_l \in \mathbb{R}, \phi_l \in \mathbb{R}$ and $\theta_l \in \mathbb{R}$ denote delay, AoA and the AoD of the lth multipath component, respectively. The quantity $\Delta f \in \mathbb{R}$ represents the subcarrier spacing of the MIMO-OFDM system. The vector $\mathbf{b}_R(\phi_l) \in \mathbb{C}^{M_R\times 1}$ denotes the receive array manifold vector for the ULA at the UE and can be defined similarly to (3). Throughout the text, we will utilize the terms CSI, CFR, and the channel matrix interchangeably.

III. AP-SIP based RADAR parameter estimation

We harness an affine precoded superimposed pilot (AP-SIP) signal for radar target parameter estimation, channel estimation and data detection. Hence, the DFRC-BS transmits an AP-SIP signal, which comprises both pilot and data signals. The DFRC BS receives the echoes as a result of reflections by multiple targets and by exploiting them it estimates the target parameters such as RCS coefficients, angle and range. Furthermore, the transmitted AP-SIP signal is also received at the UE via targets that act as potential scatterers. Subsequently, the UE exploits these for wireless channel estimation and data detection.

A. Radar parameter estimation

For reducing the complexity, frequency domain (FD) signal processing is employed, which is made possible via the *overlap and add* method. To begin with, S snapshots of the transmitted signal $\mathbf{x}(n)$ are partitioned into M blocks, where the length of each block is S', as shown in Fig. 2. Next, each sub-block and the RCS coefficients $\alpha_t(q,n')$ are padded with $R-1$ and $S'-1$ zeros, respectively, to allow both the sequences to possess an identical length $K = S' + R - 1$. A compact representation of the zero-padded transmit signal vectors and RCS vectors corresponding to the n'th snapshot in the m'th block is given by

$$\{\mathbf{x}_{m'}(n')\}_{n'=0}^{K-1} = \left\{\mathbf{x}_{m'}(0),..,\mathbf{x}_{m'}(S'-1),\underbrace{\mathbf{0},..,\mathbf{0}}_{R-1}\right\},$$

$$\{\alpha_t(q,n')\}_{n'=0}^{K-1} = \left\{\alpha_t(q,0),..,\alpha_t(q,R-1),\underbrace{\mathbf{0},..,\mathbf{0}}_{S'-1}\right\}.$$

Note that for a given bandwidth B, the range resolution is given by $\Delta R = c/2B$. Furthermore, for a given maximum range R_{max} and the FFT size K, the number of range bins R and block length S' can be set as $R = R_{max}/\Delta R$ and $S' = K - R + 1$.

The echo signal vector $\mathbf{y}_{\text{echo},m'}(n') \in \mathbb{C}^{N_R\times 1}$ received before combining and corresponding to the n'th time index of the m'th block can be expressed as

$$\mathbf{y}_{\text{echo},m'}(n') = \sum_{q=0}^{Q-1}\mathbf{a}_R(\theta_q)\mathbf{a}_T^H(\theta_q)\mathbf{F}_{\text{RF},m'}\mathbf{x}_{m'}(n') \circledast \alpha_t(q,n') + \mathbf{v}_{m'}(n'). \tag{6}$$

The FD signal received on the kth subcarrier in the m'th block can be obtained upon applying the K-point FFT operation to the received echo $\mathbf{y}_{\text{echo},m'}(n')$, which can be represented as

$$\begin{aligned}\mathbf{y}_{\text{echo},m'}[k] &= \sum_{q=0}^{Q-1}\mathbf{a}_R(\theta_q)\mathbf{a}_T^H(\theta_q)\mathbf{F}_{\text{RF},m'}\mathbf{x}_{m'}[k]\alpha_f[q,k] + \mathbf{v}_{m'}[k]\\ &= \mathbf{H}_R[k]\mathbf{F}_{\text{RF},m'}\mathbf{x}_{m'}[k] + \mathbf{v}_{m'}[k].\end{aligned} \tag{7}$$

The quantity $\alpha_f[q,k] \in \mathbb{C}$ represents the FD RCS coefficient, which is obtained via K-point FFT of the time-domain (TD) coefficients $\{\alpha_t(q,n')\}_{n'=0}^{K-1}$. In ZP-OFDM, the receiver processes the block of length $K + L_{ZP}$, corresponding to each RF chain, using the *overlap and add* technique. To this end, the block of the last L_{ZP} symbols is overlapped and summed with the block of the initial K symbols to result in a new block of length K symbols. Note that this new block of length K represents a circular convolution between the K transmit samples without ZP and the zero-padded RCS coefficients. This is subsequently processed by a K-point FFT block, as done in CP-OFDM processing.

The matrix $\mathbf{H}_R[k] \in \mathbb{C}^{N_R\times N_T}$ contains information about the angles and ranges of the targets, which can be modeled as

$$\mathbf{H}_R[k] = \sum_{q=0}^{Q-1}\alpha_f[q,k]\mathbf{a}_R(\theta_q)\mathbf{a}_T^H(\theta_q). \tag{8}$$

The above model can be expressed in the compact form as

$$\mathbf{H}_R[k] = \mathbf{A}_R\mathbf{Diag}(\widetilde{\boldsymbol{\gamma}}(k))\mathbf{A}_T^H \tag{9}$$

where $\widetilde{\boldsymbol{\gamma}}(k) \in \mathbb{C}^{Q\times 1}$, $\mathbf{A}_R \in \mathbb{C}^{N_R\times Q}$ and $\mathbf{A}_T \in \mathbb{C}^{N_T\times Q}$ denoting the receive and transmit codebooks, respectively, which can be expressed as

$$\begin{aligned}\widetilde{\boldsymbol{\gamma}}[k] &= \begin{bmatrix}\alpha_f[0,k] & \alpha_f[1,k] & ... & \alpha_f[Q-1,k]\end{bmatrix}^T,\\ \mathbf{A}_R &= \begin{bmatrix}\mathbf{a}_R(0) & \mathbf{a}_R(1) & ... & \mathbf{a}_R(Q-1)\end{bmatrix},\\ \mathbf{A}_T &= \begin{bmatrix}\mathbf{a}_T(0) & \mathbf{a}_T(1) & ... & \mathbf{a}_T(Q-1)\end{bmatrix}.\end{aligned}$$

The SIP signal used for integrated sensing and communication is described next. The BS transmits $N_F = \frac{N_T}{N_{RF}}$, frames each of length L. Thus, the total length of M transmitted blocks is LN_F. Furthermore, each frame consists of M_P/N_F and $L - (M_P/N_F)$ pilot and data vectors, respectively. The transmitted SIP matrix, corresponding to the mth frame and kth subcarrier is $\mathbf{X}_m[k] \in \mathbb{C}^{N_{RF}\times L}$, which can be modeled as

$$\mathbf{X}_m[k] = \mathbf{X}_{p,m}[k]\mathbf{P}_{p,m} + \mathbf{X}_{d,m}[k]\mathbf{P}_{d,m}, \tag{10}$$

where $\mathbf{X}_{p,m}[k] \in \mathbb{C}^{N_{RF}\times\left(\frac{M_P}{N_F}\right)}$ and $\mathbf{X}_{d,m}[k] \in \mathbb{C}^{N_{RF}\times\left(L-\frac{M_P}{N_F}\right)}$ denote the pilot and data matrices, respectively, in the mth frame. Furthermore, $\mathbf{P}_{p,m} \in \mathbb{C}^{\left(\frac{M_P}{N_F}\right)\times L}$ and $\mathbf{P}_{d,m} \in \mathbb{C}^{\left(L-\frac{M_P}{N_F}\right)\times L}$ denote the pilot and data precoding matrices for the mth frame. The data symbols are drawn from a constellation having an average symbol power of ρ_d, which leads to the property

$$\mathbb{E}\left[\mathbf{X}_{d,m}[k]\mathbf{X}_{d,m}^H[k]\right] = \left(L - \frac{M_P}{N_F}\right)\rho_d\mathbf{I}_{N_{RF}}. \tag{11}$$

The average pilot power is fixed as

$$\rho_c = \frac{\text{Tr}\left(\mathbf{X}_{p,m}[k]\mathbf{X}_{p,m}^H[k]\right)}{N_{RF}\times\frac{M_P}{N_F}}, \tag{12}$$

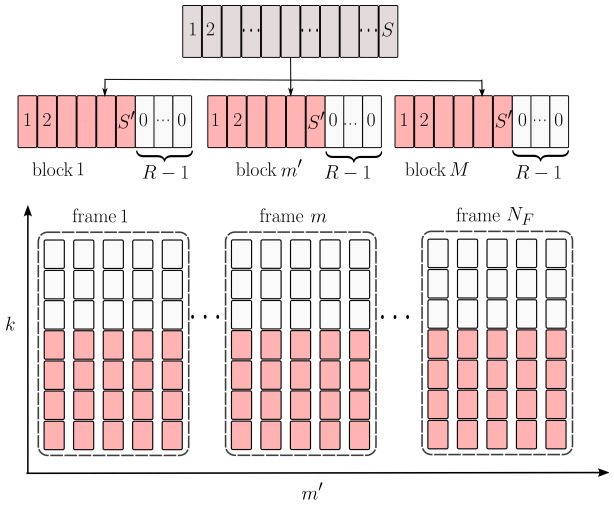

FIGURE 2: Snapshots to frames formation

so that $\rho_c + \rho_d = 1$. The received signal matrix $\widetilde{\mathbf{Y}}_m[k] \in \mathbb{C}^{N_R \times L}$ corresponding to the mth transmitted frame, can be formulated as

$$\widetilde{\mathbf{Y}}_{\text{echo},m}[k] = \mathbf{H}_R[k]\mathbf{F}_{\text{RF},m}\mathbf{X}_m[k] + \widetilde{\mathbf{V}}_m[k], \tag{13}$$

where $\mathbf{F}_{\text{RF},m} \in \mathbb{C}^{N_T \times N_{RF}}$ represents the frequency-flat RF TPC for the mth frame and $\widetilde{\mathbf{V}}_m[k] \in \mathbb{C}^{N_R \times L}$ denotes the AWGN matrix with distribution $\mathcal{CN}(0, \sigma_v^2 \mathbf{I}_{N_R})$. Next, upon concatenating all the N_F frames, the output matrix $\widetilde{\mathbf{Y}}_{\text{echo}}[k] = \left[\widetilde{\mathbf{Y}}_{\text{echo},1}[k], \widetilde{\mathbf{Y}}_{\text{echo},2}[k], .., \widetilde{\mathbf{Y}}_{\text{echo},N_F}[k]\right] \in \mathbb{C}^{N_R \times LN_F}$ can be expressed as

$$\widetilde{\mathbf{Y}}_{\text{echo}}[k] = \mathbf{H}_R[k]\mathbf{F}_{\text{RF}}\mathbf{X}[k] + \widetilde{\mathbf{V}}[k], \tag{14}$$

where $\mathbf{F}_{\text{RF}} = [\mathbf{F}_{\text{RF},1}, \mathbf{F}_{\text{RF},2}, .., \mathbf{F}_{\text{RF},N_F}] \in \mathbb{C}^{N_T \times N_T}$ and $\widetilde{\mathbf{V}}[k] = \left[\widetilde{\mathbf{V}}_1[k], \widetilde{\mathbf{V}}_2[k], ..., \widetilde{\mathbf{V}}_{N_F}[k]\right] \in \mathbb{C}^{N_R \times LN_F}$ denote the concatenated RF TPC and noise matrices, respectively. Furthermore, $\mathbf{X}[k] = \text{blkdiag}\left(\mathbf{X}_1[k], \mathbf{X}_2[k], .., \mathbf{X}_{N_F}[k]\right) \in \mathbb{C}^{N_T \times LN_F}$ represents the block diagonal SIP matrix corresponding to the kth subcarrier.

Let $N_{CF} = \frac{N_R}{N_{RF}}$ denote the number of combining frames. Each combining frame is combined using N_C/N_{CF} combining vectors. After receive combining, the output matrix $\breve{\mathbf{Y}}_q[k] \in \mathbb{C}^{(N_C/N_{CF}) \times LN_F}$, corresponding to the qth combining frame, can be expressed as

$$\breve{\mathbf{Y}}_q[k] = \mathbf{W}_{\text{BB},q}^H[k]\mathbf{W}_{\text{RF},q}^H\widetilde{\mathbf{Y}}_{\text{echo}}[k]. \tag{15}$$

Next, the final output matrix $\mathbf{Y}_{\text{echo}}[k] = \left[\breve{\mathbf{Y}}_1^T[k], \breve{\mathbf{Y}}_2^T[k], ..., \breve{\mathbf{Y}}_{N_{CF}}^T[k]\right]^T \in \mathbb{C}^{N_C \times LN_F}$ obtained after concatenation of $\breve{\mathbf{Y}}_q[k]$ across all the N_{CF} frames can be written as

$$\mathbf{Y}_{\text{echo}}[k] = \mathbf{W}_{\text{BB}}^H[k]\mathbf{W}_{\text{RF}}^H\mathbf{H}_R[k]\mathbf{F}_{\text{RF}}\mathbf{X}[k] + \mathbf{V}[k], \tag{16}$$

where $\mathbf{W}_{\text{RF}} = [\mathbf{W}_{\text{RF},1}, \mathbf{W}_{\text{RF},2}, ..., \mathbf{W}_{\text{RF},N_{CF}}] \in \mathbb{C}^{N_R \times N_R}$ is the concatenated frequency-flat RF RC matrix and $\mathbf{W}_{\text{BB}}[k] = \text{blkdiag}\left[\mathbf{W}_{\text{BB},1}[k], \mathbf{W}_{\text{BB},2}[k], ..., \mathbf{W}_{\text{BB},N_{CF}}[k]\right] \in \mathbb{C}^{N_R \times N_C}$ represents the frequency-selective baseband block-diagonal matrix. The quantity $\mathbf{V}[k] = \mathbf{W}^H[k]\widetilde{\mathbf{V}}[k] \sim \mathcal{CN}\left(0, \sigma_v^2 \mathbf{W}^H[k]\mathbf{W}[k]\right) \in \mathbb{C}^{N_R \times LN_F}$ denotes the combined noise matrix, where $\mathbf{W}[k] = \mathbf{W}_{\text{RF}}\mathbf{W}_{\text{BB}}[k]$. It is important to note that baseband precoding, $\bar{\mathbf{F}}_{\text{BB}}$, is not utilized during the target parameter estimation and channel state information (CSI) estimation of the UE. To optimize the baseband precoder, CSI information is required at the transmitter, which is not available during the training phase. This approach aligns with previous contributions, as exemplified in [14], in the context of mmWave MIMO CSI estimation. In this context, these contributions utilize only the RF precoder for CSI estimation.

Now, one can construct the block diagonal SIP matrix $\mathbf{X}[k] \in \mathbb{C}^{N_T \times LN_F}$ as

$$\mathbf{X}[k] = \mathbf{X}_p[k]\mathbf{P}_p + \mathbf{X}_d[k]\mathbf{P}_d, \tag{17}$$

where $\mathbf{X}_p[k] \in \mathbb{C}^{N_T \times M_P}$ and $\mathbf{X}_d[k] \in \mathbb{C}^{N_T \times (LN_F - M_P)}$ are the block-diagonal pilot and data matrices, which can be expressed as

$$\begin{aligned} \mathbf{X}_p[k] &= \text{blkdiag}\left(\mathbf{X}_{p,1}[k], \mathbf{X}_{p,2}[k], .., \mathbf{X}_{p,N_{CF}}[k]\right), \\ \mathbf{X}_d[k] &= \text{blkdiag}\left(\mathbf{X}_{d,1}[k], \mathbf{X}_{d,2}[k], .., \mathbf{X}_{d,N_{CF}}[k]\right). \end{aligned} \tag{18}$$

Furthermore, $\mathbf{P}_p \in \mathbb{C}^{M_P \times LN_F}$ and $\mathbf{P}_d \in \mathbb{C}^{(LN_F - M_P) \times LN_F}$ represent the block-diagonal pilot and data precoding matrices, respectively, which can be expressed as

$$\begin{aligned} \mathbf{P}_p &= \text{blkdiag}\left(\mathbf{P}_p[1], \mathbf{P}_p[2], .., \mathbf{P}_p[N_c]\right), \\ \mathbf{P}_d &= \text{blkdiag}\left(\mathbf{P}_d[1], \mathbf{P}_d[2], .., \mathbf{P}_d[N_c]\right). \end{aligned} \tag{19}$$

Note that in the SIP framework, it is important to suppress the interference caused by the data matrix during the channel estimation and the pilot matrix during the data detection phases. Toward achieving this, the pilot and data precoding matrices should necessarily satisfy the following properties:

$$\begin{aligned} \mathbf{P}_p\mathbf{P}_p^H &= \mathbf{I}_{M_P}, & \mathbf{P}_p\mathbf{P}_d^H &= \mathbf{0}_{M_P \times (LN_F - M_P)}, \\ \mathbf{P}_d\mathbf{P}_d^H &= \mathbf{I}_{(LN_F - M_P)}, & \mathbf{P}_d\mathbf{P}_p^H &= \mathbf{0}_{(LN_F - M_P) \times M_P}. \end{aligned}$$

One can observe that in order to satisfy the above properties, the constituent precoding sub-matrices $\mathbf{P}_{p,m}$ and $\mathbf{P}_{d,m}$ can be selected as the first M_P/N_F rows and the rest of the $[L - (M_P/N_F)]$ rows to be those of any unitary matrix, respectively. The pilot and data assisted radar target parameter estimation schemes are discussed next.

1) Pilot-assisted radar (PAR) model

To estimate the radar parameters from the pilots, the received echo matrix is post-multiplied by $\mathbf{P}_p^H$ to decouple the pilot component as follows:

$$\breve{\mathbf{Y}}_p[k] = \mathbf{W}^H[k]\mathbf{H}_R[k]\mathbf{F}_{\text{RF}}\mathbf{X}_p[k] + \breve{\mathbf{V}}_p[k], \tag{20}$$

where $\breve{\mathbf{Y}}_p[k] = \mathbf{Y}_{\text{echo}}[k]\mathbf{P}_p^H \in \mathbb{C}^{N_C \times M_P}$ and $\breve{\mathbf{V}}_p[k] = \mathbf{V}[k]\mathbf{P}_p^H \in \mathbb{C}^{N_C \times M_P}$. Substituting now the expression of

$\mathbf{H}_R[k]$ from (9) into (20), the above model can be rewritten as

$$\check{\mathbf{Y}}_p[k] = \mathbf{W}^H[k]\mathbf{A}_R\mathbf{Diag}(\widetilde{\boldsymbol{\gamma}}[k])\mathbf{A}_T^H\mathbf{F}_{\text{RF}}\mathbf{X}_p[k] + \check{\mathbf{V}}_p[k]. \tag{21}$$

Next, performing the $\text{vec}(\cdot)$ operation and applying the property of the so-called Khatri-Rao product [37], the received echo vector can be equivalently expressed as

$$\check{\mathbf{y}}_p[k] = \boldsymbol{\Omega}_p[k]\widetilde{\boldsymbol{\gamma}}[k] + \check{\mathbf{v}}_p[k], \tag{22}$$

where $\check{\mathbf{y}}_p[k] \in \mathbb{C}^{N_C M_P \times 1}$,$\check{\mathbf{v}}_p[k] \in \mathbb{C}^{N_C M_P \times 1}$ and $\boldsymbol{\Omega}_p[k] \in \mathbb{C}^{N_C M_P \times Q}$ denotes the *pilot sensing-matrix*. The corresponding expressions can be given as

$$\begin{aligned}
&\check{\mathbf{y}}_p[k] = \text{vec}(\check{\mathbf{Y}}_p[k]),\\
&\check{\mathbf{v}}_p[k] = \text{vec}(\check{\mathbf{V}}_p[k]) \sim \mathcal{CN}(0, \sigma_v^2[\mathbf{I}_{M_P} \otimes \mathbf{W}^H[k]\mathbf{W}[k]])\\
&\boldsymbol{\Omega}_p[k] = \left(\mathbf{X}_p^T[k]\mathbf{F}_{\text{RF}}^T\mathbf{A}_T^* \odot \mathbf{W}^H[k]\mathbf{A}_R\right).
\end{aligned} \tag{23}$$

Let $\boldsymbol{\Gamma}_t \in \mathbb{C}^{Q\times R}$ denote the TD RCS matrix whose (q,r)th entries are represented by $\alpha_t(q,r)$. One can obtain the FD RCS matrix $\boldsymbol{\Gamma}_f \in \mathbb{C}^{Q\times K}$ from $\boldsymbol{\Gamma}_t$ using the relationship of - $\boldsymbol{\Gamma}_f = \begin{bmatrix}\boldsymbol{\Gamma}_t & \mathbf{0}\end{bmatrix}\mathbf{F}^T$, where $\mathbf{F} \in \mathbb{C}^{K\times K}$ represents the DFT matrix. The expression can be simplified as

$$\boldsymbol{\Gamma}_f = \boldsymbol{\Gamma}_t\mathbf{F}_1^T, \tag{24}$$

where $\mathbf{F}_1 \in \mathbb{C}^{K\times R}$ represents the first R columns of $\mathbf{F}$. Thus, by vectorizing (24), one obtains the relationship:

$$\boldsymbol{\gamma}_f = \widetilde{\mathbf{F}}_1\boldsymbol{\gamma}_t, \tag{25}$$

where $\boldsymbol{\gamma}_f = \left[\tilde{\boldsymbol{\gamma}}^T[1], \tilde{\boldsymbol{\gamma}}^T[2], .., \tilde{\boldsymbol{\gamma}}^T[K]\right]^T = \text{vec}(\boldsymbol{\Gamma}_f) \in \mathbb{C}^{QK\times 1}$ is FD RCS vector, $\widetilde{\mathbf{F}}_1 = (\mathbf{F}_1 \otimes \mathbf{I}_Q) \in \mathbb{C}^{QK\times QR}$. The quantity $\boldsymbol{\gamma}_t = \text{vec}(\boldsymbol{\Gamma}_t) \in \mathbb{C}^{QR\times 1}$ is TD RCS vector obtained via vectorization of the TD RCS matrix $\boldsymbol{\Gamma}_t$. Stacking $\check{\mathbf{y}}_p[k]$ across all the subcarriers, the received vector $\mathbf{y}_p = [\check{\mathbf{y}}_p^T[1], \check{\mathbf{y}}_p^T[2], .., \check{\mathbf{y}}_p^T[K]]^T \in \mathbb{C}^{KN_C M_P\times 1}$ can be modeled as

$$\mathbf{y}_p = \boldsymbol{\Omega}_p\boldsymbol{\gamma}_f + \mathbf{v}_p, \tag{26}$$

where $\mathbf{v}_p = [\check{\mathbf{v}}_p^T[1], \check{\mathbf{v}}_p^T[2], .., \check{\mathbf{v}}_p^T[K]]^T$ is distributed as $\mathcal{CN}(0, \mathbf{R}_{v,p})$ and is of size $\mathbb{C}^{KN_C M_P\times 1}$. The matrix $\boldsymbol{\Omega}_p = \text{blkdiag}\left(\boldsymbol{\Omega}_p[1], \boldsymbol{\Omega}_p[2], .., \boldsymbol{\Omega}_p[K]\right) \in \mathbb{C}^{KN_C M_P\times QK}$. Leveraging the relationship in (25), one obtains the pilot-assisted radar input-output model

$$\mathbf{y}_p = \boldsymbol{\Phi}_p\boldsymbol{\gamma}_t + \mathbf{v}_p, \tag{27}$$

where $\boldsymbol{\Phi}_p = \boldsymbol{\Omega}_p\widetilde{\mathbf{F}}_1 \in \mathbb{C}^{KN_C M_P\times QR}$ is the *pilot sensing matrix*. Since this is a linear model, one can obtain the best linear unbiased estimate (BLUE) of $\boldsymbol{\gamma}_t$ employing the popular least squares (LS) technique, which is given as $\widehat{\boldsymbol{\gamma}}_t^{LS} = \boldsymbol{\Phi}_p^{\dagger}\mathbf{y}_p$. Similarly, the minimum mean square error (MMSE) estimate can be derived as

$$\widehat{\boldsymbol{\gamma}}_t^{MMSE} = \left(\boldsymbol{\Phi}_p^H\mathbf{R}_{v,p}^{-1}\boldsymbol{\Phi}_p + \mathbf{R}_{\gamma}^{-1}\right)^{-1}\boldsymbol{\Phi}_p^H\mathbf{R}_{v,p}^{-1}\mathbf{y}_p, \tag{28}$$

where the covariance matrices ovey $\mathbf{R}_{\gamma} = \mathbb{E}\left\{\boldsymbol{\gamma}_t\boldsymbol{\gamma}_t^H\right\} \in \mathbb{C}^{QR\times QR}$ and $\mathbf{R}_{v,p} = \sigma_v^2\left[\mathbf{I}_{KM_P} \otimes \mathbf{W}^H[k]\mathbf{W}[k]\right]$. At this juncture, it is important to note that the data symbols are also known at the DFRC BS. Furthermore, in a frame, the number of data symbols $L - M_P/N_F$ is large in comparison to the number of pilot symbols, which equals M_P/N_F. Thus, one can develop a more robust radar parameter estimation model by incorporating the increased number of observations corresponding to the data symbols, which can lead to a significant boost in the accuracy of target parameter estimation. Toward this end, the data-assisted radar model is presented next.

2) Data-assisted radar (DAR) model

One can obtain the data-assisted radar model by post-multiplying the echo $\mathbf{Y}_{\text{echo}}[k]$ with $\mathbf{P}_d^H$ as

$$\check{\mathbf{Y}}_d[k] = \mathbf{W}^H[k]\mathbf{A}_R\mathbf{Diag}(\widetilde{\boldsymbol{\gamma}}[k])\mathbf{A}_T^H\mathbf{F}_{\text{RF}}\mathbf{X}_d[k] + \check{\mathbf{V}}[k], \tag{29}$$

where $\check{\mathbf{Y}}_d[k] = \mathbf{Y}_{\text{echo}}[k]\mathbf{P}_d^H \in \mathbb{C}^{N_C\times(LN_F - M_P)}$ and $\check{\mathbf{V}}[k] = \mathbf{V}[k]\mathbf{P}_d^H \in \mathbb{C}^{N_C\times(LN_F - M_P)}$. Applying the $\text{vec}(\cdot)$ operation to the observation matrix of (29) yields the vectorized observation $\check{\mathbf{y}}_d[k] \in \mathbb{C}^{N_C(LN_F - M_P)\times 1}$ as

$$\check{\mathbf{y}}_d[k] = \boldsymbol{\Omega}_d[k]\widetilde{\boldsymbol{\gamma}}[k] + \check{\mathbf{v}}_d[k], \tag{30}$$

where $\boldsymbol{\Omega}_d[k] \in \mathbb{C}^{N_C(LN_F - M_P)\times Q}$ and $\check{\mathbf{v}}_d[k] \in \mathbb{C}^{N_C(LN_F - M_P)\times 1}$. The corresponding expressions can be given as

$$\begin{aligned}
&\boldsymbol{\Omega}_d[k] = \left(\mathbf{X}_d^T[k]\mathbf{F}_{\text{RF}}^T\mathbf{A}_{\text{T}}^* \odot \mathbf{W}^H\mathbf{A}_{\text{R}}\right)\\
&\check{\mathbf{v}}_d[k] \sim \mathcal{CN}(0, \sigma_v^2[\mathbf{I}_{(LN_F - M_P)} \otimes \mathbf{W}^H[k]\mathbf{W}[k]])
\end{aligned} \tag{31}$$

Stacking the vectors $\check{\mathbf{y}}_d[k]$, across all the subcarriers, one can obtain the FD input-output model for the RCS vector $\boldsymbol{\gamma}_f$ as

$$\mathbf{y}_d = \boldsymbol{\Omega}_d\boldsymbol{\gamma}_f + \mathbf{v}_d, \tag{32}$$

where $\mathbf{y}_d \in \mathbb{C}^{KN_C(LN_F - M_P)\times 1}$ and $\mathbf{v}_d \in \mathbb{C}^{KN_C(LN_F - M_P)\times 1}$. The corresponding expressions can be given as

$$\begin{aligned}
&\mathbf{y}_d = [\check{\mathbf{y}}_d^T[1], \check{\mathbf{y}}_d^T[2], .., \check{\mathbf{y}}_d^T[K]]^T\\
&\mathbf{v}_d = [\check{\mathbf{v}}_d^T[1], \check{\mathbf{v}}_d^T[2], .., \check{\mathbf{v}}_d^T[K]]^T \sim \mathcal{CN}(0, \mathbf{R}_{v,d}).
\end{aligned} \tag{33}$$

The noise covariance matrix obeys

$$\mathbf{R}_{v,d} = \sigma_v^2[\mathbf{I}_{KN_C(LN_F - M_P)} \otimes \mathbf{W}^H[k]\mathbf{W}[k]]. \tag{34}$$

The matrix $\boldsymbol{\Omega}_d = \text{blkdiag}\left(\boldsymbol{\Omega}_d[1], \boldsymbol{\Omega}_d[2], .., \boldsymbol{\Omega}_d[K]\right) \in \mathbb{C}^{KN_C(LN_F - M_P)\times QK}$. Similar to the pilot-assisted radar model, the data-assisted radar model constructed for the estimation of the TD RCS vector can be formulated as

$$\mathbf{y}_d = \boldsymbol{\Phi}_d\boldsymbol{\gamma}_t + \mathbf{v}_d, \tag{35}$$

where $\boldsymbol{\Phi}_d = \boldsymbol{\Omega}_d\widetilde{\mathbf{F}}_1 \in \mathbb{C}^{KN_C(LN_F - M_P)\times QR}$ is the *data sensing matrix*. One can observe that in both the PAR and DAR models of (27) and (35), respectively, the observation vectors and the sensing matrices of both the systems are available at the DFRC BS. Thus, one can jointly exploit the information from both the PAR and DAR models for enhanced parameter estimation accuracy, which is described next.

3) Joint pilot-data radar (JPDR) model

For improved parameter estimation, one can stack the output vectors $\mathbf{y}_p$ and $\mathbf{y}_d$ from (27) and (35), respectively, to obtain the model

$$\mathbf{y}_j = \mathbf{\Phi}_j \boldsymbol{\gamma}_t + \mathbf{v}_j, \tag{36}$$

where the above-mentioned terms can be defined as

$$\underbrace{\begin{bmatrix}\mathbf{y}_p\\ \mathbf{y}_d\end{bmatrix}}_{\substack{\mathbf{y}_j\in\\ \mathbb{C}^{KN_CLN_F\times 1}}} = \underbrace{\begin{bmatrix}\mathbf{\Phi}_p\\ \mathbf{\Phi}_d\end{bmatrix}}_{\substack{\mathbf{\Phi}_j\in\\ \mathbb{C}^{KN_CLN_F\times QR}}} \boldsymbol{\gamma}_t + \underbrace{\begin{bmatrix}\mathbf{v}_p\\ \mathbf{v}_d\end{bmatrix}}_{\substack{\mathbf{v}_j\in\\ \mathbb{C}^{KN_CLN_F\times 1}}}, \tag{37}$$

where $\mathbf{v}_j$ denotes the noise vector that is distributed as $\mathcal{CN}(0, \mathbf{R}_j)$, and the covariance matrix $\mathbf{R}_j = \text{blkdiag}(\mathbf{R}_{v,p}, \mathbf{R}_{v,d})$. The matrix $\mathbf{\Phi}_j$ is the *joint-sensing matrix*. It is important to note that typically very few targets ($L_t \ll QR$) are present in the scattering scene; consequently, there are very few non-zero values in the TD RCS matrix $\mathbf{\Gamma}_t$. Therefore, $\mathbf{\Gamma}_t$ is a sparse matrix and its vectorized version, $\boldsymbol{\gamma}_t$, is a sparse vector. Although, the system models in (27), (35) and (36) are linear in nature, conventional RCS estimation approaches such as the best linear unbiased estimator (BLUE) and MMSE lead to poor performance. This is due to the fact that these schemes do not exploit the sparsity of $\boldsymbol{\gamma}_t$. Therefore, these problems are sparse recovery problems and consequently, techniques such as OMP can be utilized for solving them effectively. However, the performance of OMP is sensitive both to the choice of the threshold and of the sensing matrix. In this context, the Bayesian learning framework proposed in [38] has shown excellent performance for sparse signal recovery, which is described next for radar parameter estimation.

B. J-BL for radar RCS parameter matrix estimation

In the joint Bayesian learning framework (J-BL) of the sparse signal recovery, the RCS coefficient vector $\boldsymbol{\gamma}_t$ is assigned the parameterized Gaussian prior

$$p(\boldsymbol{\gamma}_t; \mathbf{\Lambda}) = \prod_{l=1}^{QR} \frac{1}{\pi\lambda_l} \exp\left(-\frac{|\gamma_t(l)|^2}{\lambda_l}\right). \tag{38}$$

The quantity λ_l denotes the hyperparameter corresponding to the lth element of $\boldsymbol{\gamma}_t$ that controls its prior variance. The diagonal matrix of hyperparameters is defined as $\mathbf{\Lambda} = \text{Diag}(\boldsymbol{\lambda}) \in \mathbb{R}^{QR\times QR}$, where the vector $\boldsymbol{\lambda} \in \mathbb{R}^{QR\times 1}$ is defined as

$$\boldsymbol{\lambda} = [\lambda_1, \lambda_2, .., \lambda_{QR}]^T.$$

The log-likelihood $\log p(\mathbf{y}_j; \boldsymbol{\lambda})$ can be derived as

$$\log p(\mathbf{y}_j; \boldsymbol{\lambda}) = -\xi - \log|\mathbf{\Sigma}_{y_j}| - \mathbf{y}_j^H \Sigma_{y_j}^{-1} \mathbf{y}_j, \tag{39}$$

where $\xi = -KN_CLN_F \log(\pi)$ and $\mathbf{\Sigma}_{y_j} = (\mathbf{\Phi}_j \mathbf{\Lambda} \mathbf{\Phi}_j^H + \mathbf{R}_j) \in \mathbb{C}^{KN_CLN_F\times KN_CLN_F}$. The maximum-likelihood (ML) estimate of $\boldsymbol{\lambda}$ can now be computed as follows

$$\widehat{\boldsymbol{\lambda}}_{ML} = \arg\max_{\lambda\geq 0} \log p(\mathbf{y}_j; \boldsymbol{\lambda}). \tag{40}$$

Due to the non-concave nature of the log-likelihood function in (40), direct maximization of $\log p(\mathbf{y}_j; \boldsymbol{\lambda})$ is mathematically intractable [38]. The iterative expectation-maximization framework offers an attractive low-complexity approach to solving the above problem, which ensures convergence to a local optimum. In this algorithm, to begin with, the complete data can be defined as $\{\mathbf{y}_j, \boldsymbol{\gamma}_t\}$, where the quantity $\boldsymbol{\gamma}_t$ denotes the latent variable. Let $\widehat{\mathbf{\Lambda}}^{(j-1)}$ represent the estimate of $\mathbf{\Lambda}$ obtained in the $(j-1)$st iteration. The log-likelihood function of complete data in the expectation-step (E-step) is given by

$$\mathcal{L}\left(\mathbf{\Lambda}|\widehat{\mathbf{\Lambda}}^{(j-1)}\right) = \mathbb{E}_{\boldsymbol{\gamma}_t|\mathbf{y}_j;\widehat{\mathbf{\Lambda}}^{(j-1)}}\left\{\log p(\mathbf{y}_j, \boldsymbol{\gamma}_t; \mathbf{\Lambda})\right\}, \tag{41}$$

which can be simplified to

$$\mathcal{L}\left(\mathbf{\Lambda}|\widehat{\mathbf{\Lambda}}^{(j-1)}\right) = \mathbb{E}\left\{\log\left[p\left(\boldsymbol{\gamma}_t; \mathbf{\Lambda}\right)\right]\right\} + \mathbb{E}\left\{\log\left[p\left(\mathbf{y}_j|\boldsymbol{\gamma}_t\right)\right]\right\}. \tag{42}$$

Evaluation of the above expectation requires computation of the *a posterior* density function of the parameter vector $\boldsymbol{\gamma}_t$, which can be formulated as

$$p\left(\boldsymbol{\gamma}_t|\mathbf{y}_j; \widehat{\mathbf{\Lambda}}^{(j-1)}\right) = \mathcal{CN}\left(\widehat{\boldsymbol{\gamma}}_t^{(j)}, \mathbf{\Sigma}^{(j)}\right), \tag{43}$$

where $\widehat{\boldsymbol{\gamma}}_t^{(j)}$ and $\mathbf{\Sigma}_r^{(j)}$ are expressed as

$$\begin{aligned}\widehat{\boldsymbol{\gamma}}_t^{(j)} &= \mathbf{\Sigma}^{(j)} \mathbf{\Phi}_j^H \mathbf{R}_j^{-1} \mathbf{y}_j,\\ \mathbf{\Sigma}_r^{(j)} &= \left(\mathbf{\Phi}_j^H \mathbf{R}_j^{-1} \mathbf{\Phi}_j + \left(\widehat{\mathbf{\Lambda}}^{(j-1)}\right)^{-1}\right)^{-1}.\end{aligned} \tag{44}$$

Subsequently, the log likelihood function $\mathcal{L}\left(\mathbf{\Lambda}|\widehat{\mathbf{\Lambda}}^{(j-1)}\right)$ is maximized with respect to $\mathbf{\Lambda}$ in the maximization step (M-step). As it can be readily seen from (42), the second term $\mathbb{E}\left\{\log\left[p\left(\mathbf{y}_p|\boldsymbol{\gamma}_t\right)\right]\right\}$ is independent of the hyperparameters $\mathbf{\Lambda}$. Therefore, this can be discarded during the maximization stage. The optimization problem of the estimation of $\mathbf{\Lambda}$ in the jth iteration can be formulated as

$$\begin{aligned}\widehat{\mathbf{\Lambda}}^{(j)} &= \arg\max_{\mathbf{\Lambda}} \mathbb{E}\left\{\log\left[p(\boldsymbol{\gamma}_t; \mathbf{\Lambda})\right]\right\},\\ &= \arg\max_{\mathbf{\Lambda}} \sum_{l=1}^{QR}\left(-\log\left(\pi\lambda_l\right) - \frac{\mathbb{E}_{\boldsymbol{\gamma}_t|\mathbf{y}_j;\widehat{\mathbf{\Lambda}}^{(j-1)}}\left\{|\gamma_t(l)|^2\right\}}{\lambda_l}\right).\end{aligned} \tag{45}$$

It is important to highlight that when multiple closely spaced targets exist within the same angle-range bin, they are treated as a single-point target. Consequently, the RCS coefficients associated with different angle-range bins are considered independent. Hence, as a result of this independence, the maximization of the $\mathbf{\Lambda}$ in (45) can be decoupled with respect to each λ_l as

$$\widehat{\lambda}_l^{(j)} = \arg\max_{\lambda_l}\left(-\log\left(\pi\lambda_l\right) - \frac{\mathbb{E}_{\boldsymbol{\gamma}_t|\mathbf{y}_j;\widehat{\mathbf{\Lambda}}^{(j-1)}}\left\{|\gamma_t(l)|^2\right\}}{\lambda_l}\right). \tag{46}$$

Algorithm 1: Joint Bayesian leaning (J-BL) based RCS matrix estimation

Input: Joint observation vector $\mathbf{y}_j$, joint-sensing matrix $\mathbf{\Phi}_j$, noise covariance matrix $\mathbf{R}_j$ and stopping threshold δ and $\kappa_{\max}$

Initialization:

• Hyperparameters $\widehat{\lambda}_l^{(0)} = 1, \ \forall \ 1 \leq l \leq QR$ i.e. Hyperparameter matrix $\widehat{\mathbf{\Lambda}}^{(0)} = \mathbf{I}_{QR}$.

• Set counter variable $j = 0$, and

• $\widehat{\mathbf{\Lambda}}^{(-1)} = \mathbf{0}_{QR}$.

while, $||\widehat{\mathbf{\Lambda}}^{(j)} - \widehat{\mathbf{\Lambda}}^{(j-1)}||_F^2 > \delta$ and $j < \kappa_{max}$ **do**

$j \leftarrow j + 1$,

E-Step: Evaluate the *a posteriori* covariance and mean

$$\mathbf{\Sigma}_r^{(j)} = \left(\mathbf{\Phi}_j^H \mathbf{R}_j^{-1} \mathbf{\Phi}_j + \left(\widehat{\mathbf{\Lambda}}^{(j-1)} \right)^{-1} \right)^{-1}$$

$$\widehat{\gamma}_t^{(j)} = \mathbf{\Sigma}^{(j)} \mathbf{\Phi}_j^H \mathbf{R}_j^{-1} \mathbf{y}_j$$

M-Step: Update the hyperparameters

$$\widehat{\lambda}_l^{(j)} = \mathbf{\Sigma}^{(j)}(l,l) + \left| \widehat{\gamma}_t^{(j)}(l) \right|^2$$

end while

Output: $\widehat{\gamma}_t$

Solving the above problem via setting the gradient with respect to λ_l to zero, the estimate of the hyperparameters λ_l in the jth iteration is given by

$$\widehat{\lambda}_l^{(j)} = \mathbb{E}_{\boldsymbol{\gamma}_t | \mathbf{y}_j; \widehat{\mathbf{\Lambda}}^{(j-1)}} \left\{ |\gamma_t(l)|^2 \right\}. \tag{47}$$

The hyperparameter update in (47) can be formulated as

$$\widehat{\lambda}_l^{(j)} = \mathbf{\Sigma}^{(j)}(l,l) + \left| \widehat{\gamma}_t^{(j)}(l) \right|^2. \tag{48}$$

The E-step and M-step above are repeated for $\kappa_{\max}$ iterations or $||\widehat{\mathbf{\Lambda}}^{(j)} - \widehat{\mathbf{\Lambda}}^{(j-1)}||_F^2 \leq \delta$, whichever occurs first, where the SBL parameters $\kappa_{\max}$ and δ are chosen judiciously for precise estimation. A concise summary of the various steps involved in the proposed J-BL technique for RCS parameter estimation is given in Algorithm-1. The estimated TD RCS matrix $\mathbf{\Gamma}_t$ can be expressed as

$$\widehat{\mathbf{\Gamma}}_t = \text{vec}^{-1} \left(\widehat{\gamma}_t \right),$$

wherein the $QR \times 1$ vector $\widehat{\gamma}_t$ is reshaped into the $Q \times R$ matrix $\widehat{\mathbf{\Gamma}}_t$.

Note that the AP-SIP signal is for communication purposes which we have exploited for radar parameter estimation at the DFRC BS. Using the same AP-SIP signal, the UE estimates the channel and decodes the data. This fulfils the aim of unifying the radar and communication signal processing tasks in the ISAC system. The next section develops the sparse communication channel estimation model.

IV. AP-SIP based Communication Channel estimation

The UE exploits the echoes from the L_t scatterers to obtain the CSI estimate, which is subsequently used for decoding the data symbols as well. In this regard, a sparse recovery problem is formulated for channel estimation that exploits the simultaneous sparsity over all the subcarriers. Let the quantized sets of spatial angles for the AoA and AoD spaces, Φ_R and Θ_T, respectively, be constructed as

$$\Phi_R = \left\{ \phi_p : \phi_p = \frac{\pi}{P}(p-1) - 1, \ 1 \leq p \leq P \right\}, \tag{49}$$

$$\Theta_T = \left\{ \theta_q : \theta_q = \frac{\pi}{Q}(q-1) - 1, \ 1 \leq q \leq Q \right\}, \tag{50}$$

where P and Q are the respective grid sizes. Therefore, the transmit and receive array response dictionaries for the communication sub-system are formulated as

$$\mathbf{A}_T(\Theta_T) = [\mathbf{a}_T(\theta_1), \mathbf{a}_T(\theta_2), \ldots, \mathbf{a}_T(\theta_Q)] \in \mathbb{C}^{N_T \times Q},$$

$$\mathbf{B}_R(\Phi_R) = [\mathbf{b}_R(\phi_1), \mathbf{b}_R(\phi_2), \ldots, \mathbf{b}_R(\phi_P)] \in \mathbb{C}^{M_R \times P}.$$

One can relate the CFR matrix $\mathbf{H}_f[k]$ to the beamspace CFR matrix $\mathbf{H}_{b,f}[k] \in \mathbb{C}^{P \times Q}$ [14], [39] using the relationship:

$$\mathbf{H}_f[k] = \mathbf{A}_R(\Phi_R) \mathbf{H}_{b,f}[k] \mathbf{A}_T^H(\Theta_T). \tag{51}$$

The CFR vector corresponding to the kth subcarrier $\mathbf{h}_f[k] \in \mathbb{C}^{M_R N_T \times 1}$ can now be derived by vectorize the $\mathbf{H}_f[k]$ and exploiting the property of the Kronecker-product as

$$\mathbf{h}_f[k] = \mathbf{\Psi} \mathbf{h}_{b,f}[k], \tag{52}$$

where $\mathbf{\Psi} = (\mathbf{B}_R(\Phi_R) \otimes \mathbf{A}_T^H(\Theta_T)) \in \mathbb{C}^{M_R N_T \times PQ}$ is the *sparsifying-dictionary* and $\mathbf{h}_{b,f}[k] = \text{vec}(\mathbf{H}_{b,f}[k]) \in \mathbb{C}^{PQ \times 1}$ is the beamspace CFR vector. Consequently, the output corresponding to the mth frame of the SIP signal, prior to combining at the receiver, is expressed as

$$\widetilde{\mathbf{Y}}_{\text{UE},m}[k] = \mathbf{H}_f[k] \mathbf{F}_{\text{RF},m} \mathbf{X}_m[k] + \widetilde{\mathbf{Z}}_m[k]. \tag{53}$$

Applying a procedure similar to the one carried out in (13) to (16), one can obtain the end-to-end communication system model for $\mathbf{Y}_{\text{UE}}[k] \in \mathbb{C}^{M_{CU} \times L N_F}$ as

$$\mathbf{Y}_{\text{UE}}[k] = \mathbf{U}_{\text{BB}}^H[k] \mathbf{U}_{\text{RF}}^H \mathbf{H}_f[k] \mathbf{F}_{\text{RF}} \mathbf{X}[k] + \mathbf{Z}[k], \tag{54}$$

where M_{CU} is the number of RC vectors at the UE and $M_{CF} = \frac{M_R}{M_{RF}}$ represents the number of RC frames at the UE. The matrix $\mathbf{U}_{\text{RF}}$ is defined as

$$\mathbf{U}_{\text{RF}} = [\mathbf{U}_{\text{RF},1}, \mathbf{U}_{\text{RF},2}, \ldots, \mathbf{U}_{\text{RF},M_{CF}}] \in \mathbb{C}^{M_R \times M_R},$$

$$\mathbf{U}_{\text{BB}}[k] = \text{blkdiag}\left(\mathbf{U}_{\text{BB},1}[k], \ldots, \mathbf{U}_{\text{BB},M_{CF}}[k] \right) \in \mathbb{C}^{M_R \times M_{CU}}.$$

Let $\mathbf{U}[k] = \mathbf{U}_{\text{RF}} \mathbf{U}_{\text{BB}}[k] \in \mathbb{C}^{M_R \times M_{CU}}$. The distribution of the noise matrix $\mathbf{Z}[k]$ at the UE receiver is determined as $\mathcal{CN}(\mathbf{0}, \sigma_z^2 \mathbf{U}^H[k] \mathbf{U}[k]) \in \mathbb{C}^{M_{CU} \times L N_F}$. Similar to the PAR model, the output pilot matrix $\breve{\mathbf{Y}}_{\text{UE}}[k] \in \mathbb{C}^{M_{CU} \times M_P}$, after decoupling can be expressed as

$$\breve{\mathbf{Y}}_{\text{UE}}[k] = \mathbf{U}_{\text{BB}}^H[k] \mathbf{U}_{\text{RF}}^H \mathbf{H}_f[k] \mathbf{F}_{\text{RF}} \mathbf{X}_p[k] + \breve{\mathbf{Z}}[k], \tag{55}$$

where $\breve{\mathbf{Y}}_{\text{UE}}[k] = \mathbf{Y}_{\text{UE}}[k] \mathbf{P}_p^H$ and $\breve{\mathbf{Z}}[k] = \mathbf{Z}[k] \mathbf{P}_p^H \in \mathbb{C}^{M_{CU} \times M_P}$. The observation vector $\breve{\mathbf{y}}_{p,u}[k]$ obtained upon applying the vec(.) operation to $\breve{\mathbf{Y}}_{\text{UE}}[k]$, can be derived as

$$\breve{\mathbf{y}}_{p,u}[k] = \widetilde{\mathbf{\Omega}}_{p,u}[k] \mathbf{h}_f[k] + \mathbf{z}_p[k], \tag{56}$$

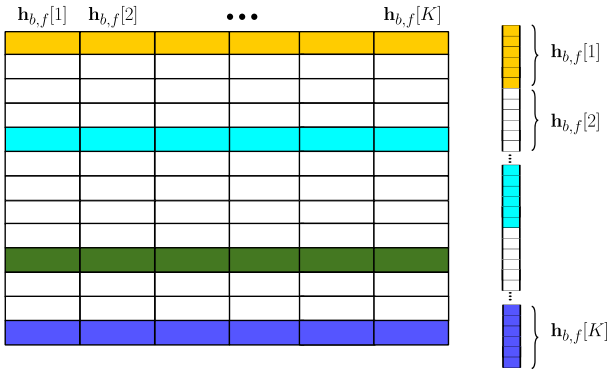

FIGURE 3: Group-sparse structure of the joint beamspace channel $\mathbf{h}_{b,f}$

where $\check{\mathbf{y}}_{p,u}[k] = \text{vec}(\check{\mathbf{Y}}_{\text{UE}}[\text{k}]) \in \mathbb{C}^{M_{CU}M_P\times 1}$, $\mathbf{z}_p[k] = \text{vec}(\check{\mathbf{Z}}[\text{k}]) \sim \mathcal{CN}(\mathbf{0}, \sigma_z^2(\mathbf{I}_{M_P} \otimes \mathbf{U}^H\mathbf{U})) \in \mathbb{C}^{M_{CU}M_P\times 1}$, $\mathbf{h}_f[k] = \text{vec}(\mathbf{H}_f[k]) \in \mathbb{C}^{M_RN_T\times 1}$ and $\widetilde{\mathbf{\Omega}}_{p,u}[k] = \left(\mathbf{X}_p^T[k]\mathbf{F}_{\text{RF}}^T \otimes \mathbf{U}_{\text{BB}}[k]^H\mathbf{U}_{\text{RF}}^H\right) \in \mathbb{C}^{M_{CU}M_P\times M_RN_T}$. Therefore, the sparse channel estimation model of the kth subcarrier can be formulated as

$$\check{\mathbf{y}}_{p,u}[k] = \mathbf{\Omega}_{p,u}[k]\mathbf{h}_{b,f}[k] + \mathbf{z}_p[k], \tag{57}$$

where $\mathbf{\Omega}_{p,u}[k] = \widetilde{\mathbf{\Omega}}_{p,u}[k]\mathbf{\Psi} = \left(\mathbf{X}_p^T[k]\mathbf{F}_{\text{RF}}^T\mathbf{A}_T^*(\Theta_T) \otimes \mathbf{U}_{\text{BB}}^H[k]\mathbf{U}_{\text{RF}}^H\mathbf{B}_R(\Phi_R)\right) \in \mathbb{C}^{M_{CU}M_P\times PQ}$. Since only the entries corresponding to the active AoA-AoD pairs are non-zero, the beamspace channel matrix $\mathbf{H}_{b,f}[k]$ is sparse in nature. This implies that (57) is once again a sparse recovery problem. Furthermore, the support set of the beamspace CFR $\mathbf{H}_{b,f}[k]$ is the same for all subcarriers ($1 \le k \le K$) [39], [40], as depicted in Fig. 3, which is termed as group sparsity. This key attribute of the wideband channel can be exploited for further enhancing the estimation performance. As the support sets of $\mathbf{h}_{b,f}[k]$ coincide for $1 \le k \le K$, one can observe the *group-sparsity* in the stacked beamspace channel, as shown in Fig. 3. Therefore, upon stacking all the observations $\check{\mathbf{y}}_{p,u}[k]$ in (57) over all the subcarriers $1 \le k \le K$, the group Bayesian learning (G-BL) model of channel estimation can be formulated as

$$\mathbf{y}_{p,u} = \mathbf{\Phi}_{p,u}\mathbf{h}_{b,f} + \mathbf{z}_p, \tag{58}$$

where $\mathbf{y}_{p,u} = [\check{\mathbf{y}}_{p,u}^T[1], \check{\mathbf{y}}_{p,u}^T[2], .., \check{\mathbf{y}}_{p,u}^T[K]]^T \in \mathbb{C}^{KM_{CU}M_P\times 1}$ is the stacked observation vector, $\mathbf{h}_{b,f} = [\mathbf{h}_{b,f}^T[1], \mathbf{h}_{b,f}^T[2], .., \mathbf{h}_{b,f}^T[K]]^T \in \mathbb{C}^{KPQ\times 1}$ is the joint beamspace channel vector and $\mathbf{z}_p = [\check{\mathbf{z}}_{p,u}^T[1], \check{\mathbf{z}}_{p,u}^T[2], .., \check{\mathbf{z}}_{p,u}^T[K]]^T \sim \mathcal{CN}(\mathbf{0}, \mathbf{R}_z) \in \mathbb{C}^{KM_{CU}M_P\times 1}$ is the noise vector. The corresponding covariance matrix of the noise $\mathbf{z}_p$ can be formulated as $\mathbf{R}_z = (\mathbf{I}_{KM_{CU}M_P} \otimes \mathbf{U}^H\mathbf{U}) \in \mathbb{C}^{KM_{CU}M_P\times KM_{CU}M_P}$. The *equivalent sensing matrix* is expressed as $\mathbf{\Phi}_{p,u} = \text{blkdiag}\{\mathbf{\Omega}_{p,u}[1], \mathbf{\Omega}_{p,u}[2], .., \mathbf{\Omega}_{p,u}[K]\} \in \mathbb{C}^{KM_{CU}M_P\times KPQ}$.

A. G-BL for communication channel estimation

The beamspace channel for the kth subcarrier $\mathbf{h}_{b,f}[k]$ is allocated the parameterized Gaussian prior probability density function

$$p(\mathbf{h}_{b,f}[k]; \mathbf{\Upsilon}) = \prod_{g=1}^{PQ} \frac{1}{\pi\upsilon_g}\exp\left(-\frac{|\mathbf{h}_{b,f}[k](g)|^2}{\upsilon_g}\right). \tag{59}$$

The quantity υ_g denotes the hyperparameter corresponding to the gth element of $\mathbf{h}_{b,f}[k]$ that controls its prior variance. The diagonal matrix of hyperparametrs is defined as $\mathbf{\Upsilon} = \text{Diag}(\boldsymbol{\upsilon}) \in \mathbb{R}^{PQ\times PQ}$, where the vector $\boldsymbol{\upsilon} \in \mathbb{R}^{PQ\times 1}$ is defined as $\boldsymbol{\upsilon} = [\upsilon_1, \upsilon_2, .., \upsilon_{PQ}]^T$. Note that the *a priori* covariance of the vector $\mathbf{h}_{b,f}[k]$ is $\mathbf{R}_h = \mathbf{\Upsilon}$, which is initially unknown. Since the sparsity profile of $\mathbf{h}_{b,f}[k]$ is identical for all the subcarriers, the prior distribution for the joint beamspace channel vector $\mathbf{h}_{b,f}$ can be formulated as

$$p(\mathbf{h}_{b,f}; \mathbf{\Upsilon}) = \prod_{k=1}^{K}\prod_{g=1}^{PQ} \frac{1}{\pi\upsilon_g}\exp\left(-\frac{|\mathbf{h}_{b,f}[k](g)|^2}{\upsilon_g}\right). \tag{60}$$

To exploit group sparsity, the same set of hyperparameters is assigned to all the groups, i.e. $1 \le k \le K$. Hence υ_g is assigned to the elements corresponding to row indices of $\{(k-1)K + g\}_{k=1}^K$ of $\mathbf{h}_{b,f}$, for all $1 \le g \le PQ$. To estimate the KPQ parameters of $\mathbf{h}_{b,f}$, the proposed G-BL method therefore requires only PQ hyperparameters, which makes the G-BL appealing for this scenario due to its lower complexity. The matrix $\mathbf{R}_z$ is the covariance matrix of the AWGN vector $\mathbf{z}_p$. Moreover, the *a priori* covariance matrix of the joint beamspace channel vector $\mathbf{h}_{b,f}$ is $\widetilde{\mathbf{R}}_h = (\mathbf{I}_K \otimes \mathbf{\Upsilon})$. The estimation of $\mathbf{h}_{b,f}$ necessitates the estimation of the hyperparameter matrix $\mathbf{\Upsilon}$. Furthermore, as the hyperparameters obeys $\upsilon_g \to 0$, all the components of $\mathbf{h}_{b,f}$ associated with the particular hyperparameter approach zero, thus leading to group sparse recovery [38]. Once again, to exploit the EM technique for ML estimation of the beamspace CFR, the complete data is represented as $\{\mathbf{y}_{p,u}, \mathbf{h}_{b,f}\}$. Furthermore, $\widehat{\mathbf{\Upsilon}}^{(j-1)}$ represents the estimate of $\mathbf{\Upsilon}$ in the $(j-1)$st EM iteration. In the E-step, the log-likelihood of the complete data can be derived as

$$\mathcal{L}\left(\mathbf{\Upsilon}|\widehat{\mathbf{\Upsilon}}^{(j-1)}\right) = \mathbb{E}_{\mathbf{h}_{b,f}|\mathbf{y}_{p,u};\widehat{\mathbf{\Upsilon}}^{(j-1)}}\left\{\log p(\mathbf{y}_{p,u}, \mathbf{h}_{b,f}; \mathbf{\Upsilon})\right\}, \tag{61}$$

which can be further expanded as

$$\begin{aligned}\mathcal{L}\left(\mathbf{\Upsilon}|\widehat{\mathbf{\Upsilon}}^{(j-1)}\right) =& \mathbb{E}\left\{\log\left[p\left(\mathbf{h}_{b,f}; \mathbf{\Upsilon}\right)\right]\right\} \\ &+ \mathbb{E}\left\{\log\left[p\left(\mathbf{y}_{p,u}|\mathbf{h}_{b,f}\right)\right]\right\}.\end{aligned} \tag{62}$$

The posterior density of $\mathbf{h}_{b,f}$ required for evaluating the expectation above is formulated as

$$p\left(\mathbf{h}_{b,f}|\mathbf{y}_{p,u}; \widehat{\mathbf{\Upsilon}}^{(j-1)}\right) = \mathcal{CN}\left(\widehat{\mathbf{h}}_{b,f}^{(j)}, \mathbf{\Sigma}^{(j)}\right), \tag{63}$$

where the expressions for $\boldsymbol{\Sigma}^{(j)}$ and $\widehat{\mathbf{h}}_{b,f}^{(j)}$ can be written as

$$\begin{aligned}\boldsymbol{\Sigma}^{(j)} &= \left(\boldsymbol{\Phi}_{p,u}^{H}\mathbf{R}_{z}^{-1}\boldsymbol{\Phi}_{p,u} + \left(\mathbf{I}_K \otimes \left(\widehat{\boldsymbol{\Upsilon}}^{(j-1)}\right)^{-1}\right)\right)^{-1}, \\ \widehat{\mathbf{h}}_{b,f}^{(j)} &= \boldsymbol{\Sigma}^{(j)}\boldsymbol{\Phi}_{p,u}^{H}\mathbf{R}_{z}^{-1}\mathbf{y}_{p,u}.\end{aligned} \tag{64}$$

Subsequently, the log-likelihood function $\mathcal{L}\left(\boldsymbol{\Upsilon}|\widehat{\boldsymbol{\Upsilon}}^{(j-1)}\right)$ is maximized with respect to $\boldsymbol{\Upsilon}$ in the maximization step (M-step). As it can be readily seen, the second term $\mathbb{E}\left\{\log\left[p\left(\mathbf{y}_{p,u}|\mathbf{h}_{b,f}\right)\right]\right\}$, the expression for which is given in (62), is independent of the hyperparameter matrix $\boldsymbol{\Upsilon}$, and can therefore be dropped at this stage. The estimate of $\boldsymbol{\Upsilon}$ in the jth iteration is obtained as the solution of the optimization problem

$$\widehat{\boldsymbol{\Upsilon}}^{(j)} = \arg\max_{\boldsymbol{\Upsilon}} \mathbb{E}\left\{\log\left[p(\mathbf{h}_{b,f};\boldsymbol{\Upsilon})\right]\right\}. \tag{65}$$

Substituting the value of $p(\mathbf{h}_{b,f};\boldsymbol{\Upsilon})$ into (65) and ignoring the terms that do not depend on $\boldsymbol{\Upsilon}$ yields

$$\widehat{\boldsymbol{\Upsilon}}^{(j)} = \arg\max_{\boldsymbol{\Upsilon}} \sum_{g=1}^{PQ}\left[-K\log(\upsilon_g) - \sum_{k=1}^{K}\frac{\mathbb{E}\left\{\left|\mathbf{h}_{b,f}[k](g)\right|^2\right\}}{\upsilon_g}\right]. \tag{66}$$

The maximization of this equation with respect to $\boldsymbol{\Upsilon}$ can be equivalently solved by maximizing with respect to each υ_g. Differentiating the above cost function with respect to each υ_g and equating to zero yields the estimate of the hyperparameter υ_g in the jth iteration as

$$\widehat{\upsilon}_g^{(j)} = \frac{1}{K}\sum_{k=1}^{K}\mathbb{E}_{\mathbf{h}_{b,f}|\mathbf{y}_{p,u};\widehat{\boldsymbol{\Upsilon}}^{(j-1)}}\left\{\left|\mathbf{h}_{b,f}[k](g)\right|^2\right\}, \tag{67}$$

where the conditional expectation can be derived as

$$\begin{aligned}\mathbb{E}\left\{\left|\mathbf{h}_{b,f}[k](g)\right|^2\right\} = &\left|\widehat{\mathbf{h}}_{b,f}^{(j)}[(k-1)K+g]\right|^2 \\ &+ \boldsymbol{\Sigma}^{(j)}[(k-1)K+g,(k-1)K+g].\end{aligned} \tag{68}$$

The hyperparameter estimate $\widehat{\upsilon}_g^{(j)}$ in the jth iteration can be obtained by exploiting (67). The above E-step and M-step are repeated until either the maximum number of iterations κ_{max} is exhausted or $||\widehat{\boldsymbol{\Upsilon}}^{(j)} - \widehat{\boldsymbol{\Upsilon}}^{(j-1)}||_F^2 \leq \delta$. The main steps of the proposed G-BL approach harnessed for the estimation of the joint beamspace channel $\mathbf{h}_{b,f}$ are succinctly summarized in Algorithm-2.

Subsequently, one can estimate the beamspace channel vector corresponding to the kth subcarrier $\mathbf{h}_{b,f}[k]$ from $\widehat{\mathbf{h}}_{b,f}$ by selecting the rows $[(k-1)PQ+1:kPQ]$ of $\widehat{\mathbf{h}}_{b,f}$. Therefore the estimated beamspace channel matrix $\widehat{\mathbf{H}}_{b,f}[k]$ for subcarrier k is ultimately determined as

$$\widehat{\mathbf{H}}_{b,f}[k] = \mathrm{vec}^{-1}\left(\widehat{\mathbf{h}}_{b,f}[k]\right).$$

The estimate of the CFR can in turn be obtained as $\widehat{\mathbf{H}}_f[k] = \boldsymbol{\Psi}\widehat{\mathbf{H}}_{b,f}[k]$. The channel estimate obtained above can now be utilized for data detection at the UE, and its low-complexity frame-wise procedure for which is discussed next.

Algorithm 2: Group Bayesian learning (G-BL) based sparse channel estimation

Input: Observation vector $\mathbf{y}_{p,u}$, equivalent sensing matrix $\boldsymbol{\Phi}_{p,u}$, noise covariance matrix $\mathbf{R}_z$ and stopping parameters δ and κ_{max}

Initialization:

- Hyperparameters $\widehat{\upsilon}_g^{(0)} = 1, \ \forall \ 1 \leq g \leq PQ$ i.e. Hyperparameter matrix $\widehat{\boldsymbol{\Upsilon}}^{(0)} = \mathbf{I}_{PQ}$.
- Set counter variable $j = 0$ and
- $\widehat{\boldsymbol{\Upsilon}}^{(-1)} = \mathbf{0}_{PQ}$.

while, $||\widehat{\boldsymbol{\Upsilon}}^{(j)} - \widehat{\boldsymbol{\Upsilon}}^{(j-1)}||_F^2 > \delta$ and $j < \kappa_{max}$ **do**

$j \leftarrow j+1$,

E-Step: Evaluate the *a posteriori* covariance and mean

$$\boldsymbol{\Sigma}^{(j)} = \left(\boldsymbol{\Phi}_{p,u}^{H}\mathbf{R}_{z}^{-1}\boldsymbol{\Phi}_{p,u} + \left(\mathbf{I}_K \otimes \left(\widehat{\boldsymbol{\Upsilon}}^{(j-1)}\right)^{-1}\right)\right)^{-1}$$

$$\widehat{\mathbf{h}}_{b,f}^{(j)} = \boldsymbol{\Sigma}^{(j)}\boldsymbol{\Phi}_{p,u}^{H}\mathbf{R}_{z}^{-1}\mathbf{y}_{p,u}$$

M-Step: Update the hyperparameters

for $g = 1, ..., PQ$ **do**

$$\begin{aligned}\widehat{\upsilon}_g^{(j)} = &\frac{1}{K}\sum_{k=1}^{K}\left|\widehat{\mathbf{h}}_{b,f}^{(j)}[(k-1)K+g]\right|^2 \\ &+ \boldsymbol{\Sigma}^{(j)}[(k-1)K+g,(k-1)K+g]\end{aligned}$$

end for

end while

Output: $\widehat{\mathbf{h}}_{b,f} = \widehat{\mathbf{h}}_{b,f}^{(j)}$

B. Downlink data detection

We commence by decoupling the data component in $\mathbf{Y}_{\mathrm{UE}}[k]$ of (54) via post multiplication with $\mathbf{P}_d^H$. The resultant output is formulated as

$$\check{\mathbf{Y}}_d^{\mathrm{UE}}[k] = \mathbf{U}_{\mathrm{BB}}^{H}[k]\mathbf{U}_{\mathrm{RF}}^{H}\mathbf{H}_f[k]\mathbf{F}_{\mathrm{RF}}\mathbf{X}_d[k] + \mathbf{Z}[k]\mathbf{P}_d^H, \tag{69}$$

where $\check{\mathbf{Y}}_d^{\mathrm{UE}}[k] = \mathbf{Y}_{\mathrm{UE}}[k]\mathbf{P}_d^H \in \mathbb{C}^{M_{CU}\times(LN_F-M_P)}$. The mth frame can be retrieved by selecting the columns $[(m-1)(L-M_P/N_F)+1 : m(L-M_P/N_F)]$ of $\check{\mathbf{Y}}_d^{\mathrm{UE}}[k]$. The output corresponding to the mth frame is then:

$$\mathbf{Y}_m^{\mathrm{UE}}[k] = \mathbf{U}_{\mathrm{BB}}^{H}[k]\mathbf{U}_{\mathrm{RF}}^{H}\mathbf{H}_f[k]\mathbf{F}_{\mathrm{RF},m}\mathbf{X}_{d,m}[k] + \mathbf{Z}_m[k], \tag{70}$$

where $\mathbf{Y}_m^{\mathrm{UE}}[k] \in \mathbb{C}^{M_{CU}\times(L-M_P/N_F)}$ and $\mathbf{Z}_m[k] \in \mathbb{C}^{M_{CU}\times(L-M_P/N_F)}$. Let $\overline{\mathbf{H}}_m[k] = \mathbf{U}_{\mathrm{BB}}^{H}[k]\mathbf{U}_{\mathrm{RF}}^{H}\mathbf{H}_f[k]\mathbf{F}_{\mathrm{RF},m} \in \mathbb{C}^{M_{CU}\times N_{RF}}$ denote the equivalent channel matrix. The MMSE data detector for this system is formulated as

$$\begin{aligned}\widehat{\mathbf{X}}_{d,m}^{\mathrm{MMSE}}[k] = &\left(\overline{\mathbf{H}}_m^{H}[k]\overline{\mathbf{H}}_m[k] + \frac{1}{\rho_d \mathrm{SNR}}\mathbf{I}_{N_{RF}}\right)^{-1} \\ &\times \overline{\mathbf{H}}_m^{H}[k]\mathbf{Y}_m^{\mathrm{UE}}[k].\end{aligned} \tag{71}$$

V. Precoders/ Combiner and Pilot optimization

This section describes the design of the optimal baseband RC and pilots. To improve the sparse estimation performance, the optimal baseband RC and pilot matrices can be obtained by minimizing the total coherence of the dictionary matrix $\mathbf{\Phi}_{p,u}$. Toward this, set the RF TPC and the RF RC as the discrete Fourier transform (DFT) matrices of size $N_T \times N_T$ and $M_R \times M_R$ [41]- [42]. Furthermore, since the matrix $\mathbf{\Phi}_{p,u}$ is block-diagonal, the total coherence minimization of $\mathbf{\Phi}_{p,u}$ reduces to minimizing the coherence of each sub-matrix $\mathbf{\Omega}_{p,u}[k] = \left(\mathbf{X}_p^T[k]\mathbf{F}_{\text{RF}}^T\mathbf{A}_T^*(\Theta_T) \otimes \mathbf{U}_{\text{BB}}^H[k]\mathbf{U}_{\text{RF}}^H\mathbf{B}_R(\Phi_R)\right)$. The total coherence of $\mathbf{\Omega}_{p,u}[k]$ is defined as

$$\boldsymbol{\mu}^t(\mathbf{\Omega}_{p,u}[k]) = \sum_{m=1}^{PQ}\sum_{m\neq n,n=1}^{PQ}\left|\mathbf{\Omega}_{p,u}[k](:,m)^H\mathbf{\Omega}_{p,u}[k](:,n)\right|^2, \tag{72}$$

which can be upper bounded as

$$\boldsymbol{\mu}^t(\mathbf{\Omega}_{p,u}[k]) \leq ||\mathbf{\Omega}_{p,u}[k]\mathbf{\Omega}_{p,u}^H[k]||_F^2. \tag{73}$$

Let $\widetilde{\mathbf{X}}[k] = \mathbf{X}_p^T[k]\mathbf{F}_{\text{RF}}^T\mathbf{A}_T^*(\Theta_T)$ and $\widetilde{\mathbf{U}}[k] = \mathbf{U}_{\text{BB}}^H[k]\mathbf{U}_{\text{RF}}^H\mathbf{B}_R(\Phi_R)$. This implies that

$$\begin{aligned}||\mathbf{\Omega}_{p,u}[k]\mathbf{\Omega}_{p,u}^H[k]||_F^2 &= ||\widetilde{\mathbf{X}}[k]\widetilde{\mathbf{X}}^H[k]||_F^2||\widetilde{\mathbf{U}}[k]\widetilde{\mathbf{U}}^H[k]||_F^2 \\ &= \frac{PQ}{M_RN_T}||\mathbf{X}_p^T[k]\mathbf{F}_{\text{RF}}^H\mathbf{F}_{\text{RF}}\mathbf{X}_p^*[k]||_F^2||\mathbf{U}^H[k]\mathbf{U}[k]||_F^2.\end{aligned} \tag{74}$$

Hence (74) can be updated as

$$\begin{aligned}||\mathbf{\Omega}_{p,u}[k]\mathbf{\Omega}_{p,u}^H[k]||_F^2 = \frac{PQ}{M_RN_T}||\mathbf{X}_p^H[k]\mathbf{X}_p[k]||_F^2|| \\ \times \mathbf{U}_{\text{BB}}^H[k]\mathbf{U}_{\text{BB}}[k]||_F^2.\end{aligned} \tag{75}$$

It is important to note that one can approximately minimize the upper bound specified in (73) rather than minimizing the total coherence $\boldsymbol{\mu}^t(\mathbf{\Omega}_{p,u}[k])$. Furthermore, $\mathbf{X}_p$ is a block-diagonal matrix as described in (18). Hence, the quantity $||\mathbf{X}_p^H[k]\mathbf{X}_p[k]||_F^2$ can be further simplified in terms of its components as

$$||\mathbf{X}_p^H[k]\mathbf{X}_p[k]||_F^2 = \sum_{m=1}^{N_F}||\mathbf{X}_{p,m}^H[k]\mathbf{X}_{p,m}[k]||_F^2. \tag{76}$$

The minimization of $||\mathbf{X}_p^H[k]\mathbf{X}_p[k]||_F^2$ can now be accomplished by minimizing $||\mathbf{X}_{p,m}^H[k]\mathbf{X}_{p,m}[k]||_F^2$. Similarly $||\mathbf{U}_{\text{BB}}^H[k]\mathbf{U}_{\text{BB}}[k]||_F^2$ can be minimized via the minimization of $||\mathbf{U}_{\text{BB},q}^H[k]\mathbf{U}_{\text{BB},q}[k]||_F^2$. Lemma-1 below derives the optimal pilot matrix $\mathbf{X}_{p,m}[k]$ corresponding to the mth frame that minimizes $||\mathbf{X}_{p,m}^H[k]\mathbf{X}_{p,m}[k]||_F^2$ subject to the average pilot power constraint given in (12).

Lemma 1: The optimal pilot submatrix $\mathbf{X}_{p,m}^\star[k]$ can be determined as the solution of the optimization problem

$$\begin{aligned}\mathbf{X}_{p,m}^\star[k] = &\underset{\mathbf{X}_{p,m}[k]}{\text{argmin}} \quad ||\mathbf{X}_{p,m}^H[k]\mathbf{X}_{p,m}[k]||_F^2 \\ &\text{s.t.} \quad \text{Tr}\left(\mathbf{X}_{p,m}[k]\mathbf{X}_{p,m}^H[k]\right) = \rho_c N_{RF}\frac{M_P}{N_F}.\end{aligned} \tag{77}$$

The corresponding closed-form solution may be expressed as

$$\mathbf{X}_{p,m}^\star[k] = \sqrt{\rho_c N_{RF}}\mathbf{Q}_1\left[\mathbf{I}_{\frac{M_P}{N_F}} \quad \mathbf{0}_{\frac{M_P}{N_F}\times\left(N_{RF}-\frac{M_P}{N_F}\right)}\right]^T\mathbf{Q}_2^H, \tag{78}$$

where $\mathbf{Q}_1 \in \mathbb{C}^{N_{RF}\times N_{RF}}$ and $\mathbf{Q}_2 \in \mathbb{C}^{\frac{M_P}{N_F}\times\frac{M_P}{N_F}}$ are arbitrary unitary matrices.

Proof: Given in Appendix A.

The optimal value of $\mathbf{U}_{\text{BB},q}[k]$ is given by the result in Lemma 2 below.

Lemma 2: The closed-form solution of the optimization problem

$$\begin{aligned}\mathbf{U}_{\text{BB},q}^\star[k] = &\underset{\mathbf{U}_{\text{BB},q}[k]}{\text{argmin}} \quad ||\mathbf{U}_{\text{BB},q}^H[k]\mathbf{U}_{\text{BB},q}[k]||_F^2 \\ &\text{s.t.} \quad ||\mathbf{U}_{\text{BB},q}[k]||_F^2 = \frac{M_{CU}}{M_{CF}}\end{aligned} \tag{79}$$

can be derived as

$$\mathbf{U}_{\text{BB},q}^\star[k] = \mathbf{Q}_3\left[\mathbf{I}_{\frac{M_{CU}}{M_{CF}}} \quad \mathbf{0}_{\frac{M_{CU}}{M_{CF}}\times\left(M_{RF}-\frac{M_{CU}}{M_{CF}}\right)}\right]^T\mathbf{Q}_4^H, \tag{80}$$

where $\mathbf{Q}_3 \in \mathbb{C}^{M_{RF}\times M_{RF}}$ and $\mathbf{Q}_4 \in \mathbb{C}^{\frac{M_{CU}}{M_{CF}}\times\frac{M_{CU}}{M_{CF}}}$ are arbitrary unitary matrices.

Proof: Similar to the proof of Lemma-1.

One can now obtain the optimal designs for $\mathbf{W}_{\text{BB}}^\star[k]$ and $\mathbf{W}_{\text{RF}}$ along similar lines. The closed-form solution derived above for the optimal pilot matrix $\mathbf{X}_p^\star[k]$ and baseband RC $\mathbf{U}_{\text{BB}}^\star[k]$ at the UE, which minimize the total coherence of the equivalent sensing matrix $\mathbf{\Phi}_{p,u}$. This enhances the performance of channel estimation, leading to improved accuracy. Similarly, the proposed optimal pilot $\mathbf{X}_p^\star[k]$ and DFRC baseband RC $\mathbf{W}_{\text{BB}}^\star[k]$ design enhance the performance of target parameter estimation through minimization of the total coherence of the joint sensing matrix $\mathbf{\Phi}_j$.

VI. Bayesian Cramer Rao Bound

A. BCRB derivation for radar parameter estimation

This section derives the BCRB for the proposed J-BL technique, this procedure may also be readily extended to obtain the analogous results for the DA-BL and PA-BL schemes as well. We start by considering the linear model in (36). The Bayesian Fisher Information matrix (BFIM) $\mathbf{J}_R \in \mathbb{C}^{QR\times QR}$ is given by [43]

$$\mathbf{J}_R = \mathbf{J}_0 + \mathbf{J}_\gamma, \tag{81}$$

where $\mathbf{J}_0 \in \mathbb{C}^{QR\times QR}$ and $\mathbf{J}_\gamma \in \mathbb{C}^{QR\times QR}$ are the BFIMs corresponding to the measurement vector $\mathbf{y}_j$ and RCS vector $\boldsymbol{\gamma}_t$, respectively, The matrices $\mathbf{J}_0$ and $\mathbf{J}_\gamma$ can be defined as

$$\begin{aligned}\mathbf{J}_0 &= -\mathbb{E}_{(\mathbf{y}_j,\boldsymbol{\gamma}_t)}\left\{\frac{\partial^2\mathcal{L}(\mathbf{y}_j|\boldsymbol{\gamma}_t)}{\partial\boldsymbol{\gamma}_t\partial\boldsymbol{\gamma}_t^H}\right\}, \\ \mathbf{J}_\gamma &= -\mathbb{E}_{\boldsymbol{\gamma}_t}\left\{\frac{\partial^2\mathcal{L}(\boldsymbol{\gamma}_t;\mathbf{\Lambda})}{\partial\boldsymbol{\gamma}_t\partial\boldsymbol{\gamma}_t^H}\right\},\end{aligned} \tag{82}$$

where $\mathcal{L}(\mathbf{y}_j|\boldsymbol{\gamma}_t) = \log p\left(\mathbf{y}_j|\boldsymbol{\gamma}_t\right)$ and $\mathcal{L}(\boldsymbol{\gamma}_t;\mathbf{\Lambda}) = \log p\left(\boldsymbol{\gamma}_t;\mathbf{\Lambda}\right)$ are the log-likelihood of the measurement and

TABLE 4: Simulation Parameters for System-1 and System-2

Parameter	System-1	System-2	Parameter	System-1	System-2
System bandwidth, B	3.2 MHz	10.24 MHz	# DFRC BS RFCs, N_{RF}	4	8
Subcarrier Spacing, Δf	100 kHz	160 kHz	# UE antenna, M_R	8	16
# subcarriers, K	32	64	# UE RFCs, M_{RF}	2	4
# OFDM blocks in a frame, L	5	20	UE angular grid, P	10	20
# pilot vectors, M_P	4	8	DFRC angular grid, Q	18	36
# DFRC Transmit/Receive antenna, N_T and N_R	16	32	DFRC range grid, R	16	32
Range resolution, $\Delta R = c/2B$	46.87 m	14.70 m	DFRC Angular resolution, $\Delta Q = \pi/Q$	10°	5°

log-prior density of the RCS vector $\boldsymbol{\gamma}_t$, which can be formulated as

$$\begin{aligned}\mathcal{L}(\mathbf{y}_j|\boldsymbol{\gamma}_t) &= \xi_1 - (\mathbf{y}_j - \boldsymbol{\Phi}_j\boldsymbol{\gamma}_t)^H\mathbf{R}_j^{-1}(\mathbf{y}_j - \boldsymbol{\Phi}_j\boldsymbol{\gamma}_t),\\ \mathcal{L}(\boldsymbol{\gamma}_t;\boldsymbol{\Lambda}) &= \xi_2 - \boldsymbol{\gamma}_t^H\boldsymbol{\Lambda}^{-1}\boldsymbol{\gamma}_t.\end{aligned} \tag{83}$$

The constant terms ξ_1 and ξ_2 are derived as

$$\begin{aligned}\xi_1 &= -KN_CLN_F\log\pi - \log\det(\mathbf{R}_j),\\ \xi_2 &= -QR\log\pi - \log\det(\boldsymbol{\Lambda}).\end{aligned} \tag{84}$$

Now, by substituting (83) and (84) into (82), one can express the BFIMs as $\mathbf{J}_0 = \boldsymbol{\Phi}_j^H\mathbf{R}_j^{-1}\boldsymbol{\Phi}_j$ and $\mathbf{J}_\gamma = \boldsymbol{\Lambda}^{-1}$. Hence, the BFIM $\mathbf{J}_R$ can be formulated as

$$\mathbf{J}_R = \boldsymbol{\Phi}_j^H\mathbf{R}_j^{-1}\boldsymbol{\Phi}_j + \boldsymbol{\Lambda}^{-1}. \tag{85}$$

Thus, the BCRB for the mean square error (MSE) of the estimation of the RCS vector $\boldsymbol{\gamma}_t$ can be expressed as

$$\text{MSE}\left(\widehat{\boldsymbol{\gamma}}_t\right) \geq \text{Tr}\left(\mathbf{J}_R^{-1}\right). \tag{86}$$

B. BCRB for CSI estimation

Similarly, the BFIM $\mathbf{J}_C \in \mathbb{C}^{PQ\times PQ}$ for the beamspace channel vector corresponding to the kth subcarrier $\mathbf{h}_{b,f}[k]$ is given as

$$\mathbf{J}_C = \mathbf{J}_P + \mathbf{J}_H. \tag{87}$$

The FIMs $\mathbf{J}_P \in \mathbb{C}^{PQ\times PQ}$ and $\mathbf{J}_H \in \mathbb{C}^{PQ\times PQ}$ correspond to the pilot measurement vector $\mathbf{y}_p^{\text{UE}}[k]$ and $\mathbf{h}_{b,f}[k]$, respectively, which are defined as

$$\begin{aligned}\mathbf{J}_P &= -\mathbb{E}_{(\mathbf{y}_p^{\text{UE}},\mathbf{h}_{b,f}[k])}\left\{\frac{\partial^2\mathcal{L}(\mathbf{y}_p^{\text{UE}}|\mathbf{h}_{b,f}[k])}{\partial\mathbf{h}_{b,f}[k]\partial\mathbf{h}_{b,f}^H[k]}\right\},\\ \mathbf{J}_H &= -\mathbb{E}_{\mathbf{h}_{b,f}[k]}\left\{\frac{\partial^2\mathcal{L}(\mathbf{h}_{b,f}[k];\boldsymbol{\Upsilon})}{\partial\mathbf{h}_{b,f}[k]\partial\mathbf{h}_{b,f}^H[k]}\right\}.\end{aligned} \tag{88}$$

Applying a procedure similar to the one employed above in Section VI-A for radar parameter estimation, one can obtain the expression for $\mathbf{J}_C$ as

$$\mathbf{J}_C = \left[\boldsymbol{\Phi}_{p,u}^H[k]\mathbf{R}_z^{-1}\boldsymbol{\Phi}_{p,u}[k] + \boldsymbol{\Upsilon}^{-1}\right]. \tag{89}$$

Thus, the BCRB for the MSE of the estimate of the beamspace channel $\mathbf{H}_{b,f}[k]$ can be expressed as

$$\text{MSE}\left(\widehat{\mathbf{H}}_{b,f}[k]\right) \geq \text{Tr}\left[\mathbf{J}_C^{-1}\right]. \tag{90}$$

The beamspace channel vector $\mathbf{h}_{b,f}[k]$ and vectorized CFR $\mathbf{h}_f[k]$ are linearly related, as upon described in (52). Exploiting this, one can determine the BCRB for the estimate of $\mathbf{H}_f[k]$, as shown below

$$\text{MSE}\left(\widehat{\mathbf{H}}_f[k]\right) \geq \text{Tr}\left[\boldsymbol{\Psi}\mathbf{J}_C^{-1}\boldsymbol{\Psi}^H\right]^{-1}. \tag{91}$$

VII. Simulation Results

This section illustrates the performance of the proposed radar target parameter estimation and wireless channel estimation in mmWave MIMO ISAC systems. We consider two different systems (System 1 and 2) with their detailed parameter values presented in Table II, where $L_t = 8$ targets are randomly distributed in the scattering environment whose TD RCS coefficients are generated as random variables with the distribution $\alpha_t(q,r) \sim \mathcal{CN}(0,1)$. The maximum ranges for System-1 and System-2 are set to $R_{max} = 749.92$ m and 470.4 m, respectively. From the available range resolution, the range bins can be calculated as $R = 16$ and 32 for System-1 and System-2, respectively. From the available FFT size K, one can calculate the block lengths as $S' = 17$ and $S' = 33$ for System-1 and System-2, respectively. Moreover, for a given maximum angle ($[0,\pi]$ for ULA), the angular resolution is given as π/Q. Therefore, for given angular grid sizes $Q = 16$ for System-1 and 32 for System-2, angular resolutions of 10° and 5°, respectively, can be achieved. The number of transmitted frames is $N_F = 4$, number of combining frames is $N_{CF} = 4$ and combining vectors is $N_C = 8$ at the DFRC receiver for both the systems. QPSK modulation is employed for the data symbols. For BL-based estimation, the stopping parameters are set to $\delta = 10^{-6}$ and $\kappa_{\max} = 50$. The regularization parameter for FOCUSS is $0.1\sigma^2$, the l_p-norm parameter is set to $p = 0.8$ with the stopping threshold $\epsilon = 10^{-6}$, and the maximum number of iterations is chosen to be $N_{\max} = 800$.

A. Radar parameter estimation

Fig. 4a and 4d compare the NMSE performance of the PA-BL, DA-BL and J-BL schemes proposed for the PAR, DAR and JPDR models, to those of the J-OMP, J-FOCUSS and J-MMSE techniques. The J-OMP, J-FOCUSS and J-MMSE techniques are the extensions of the OMP, FOCUSS and conventional MMSE algorithms, respectively, to the JPDR

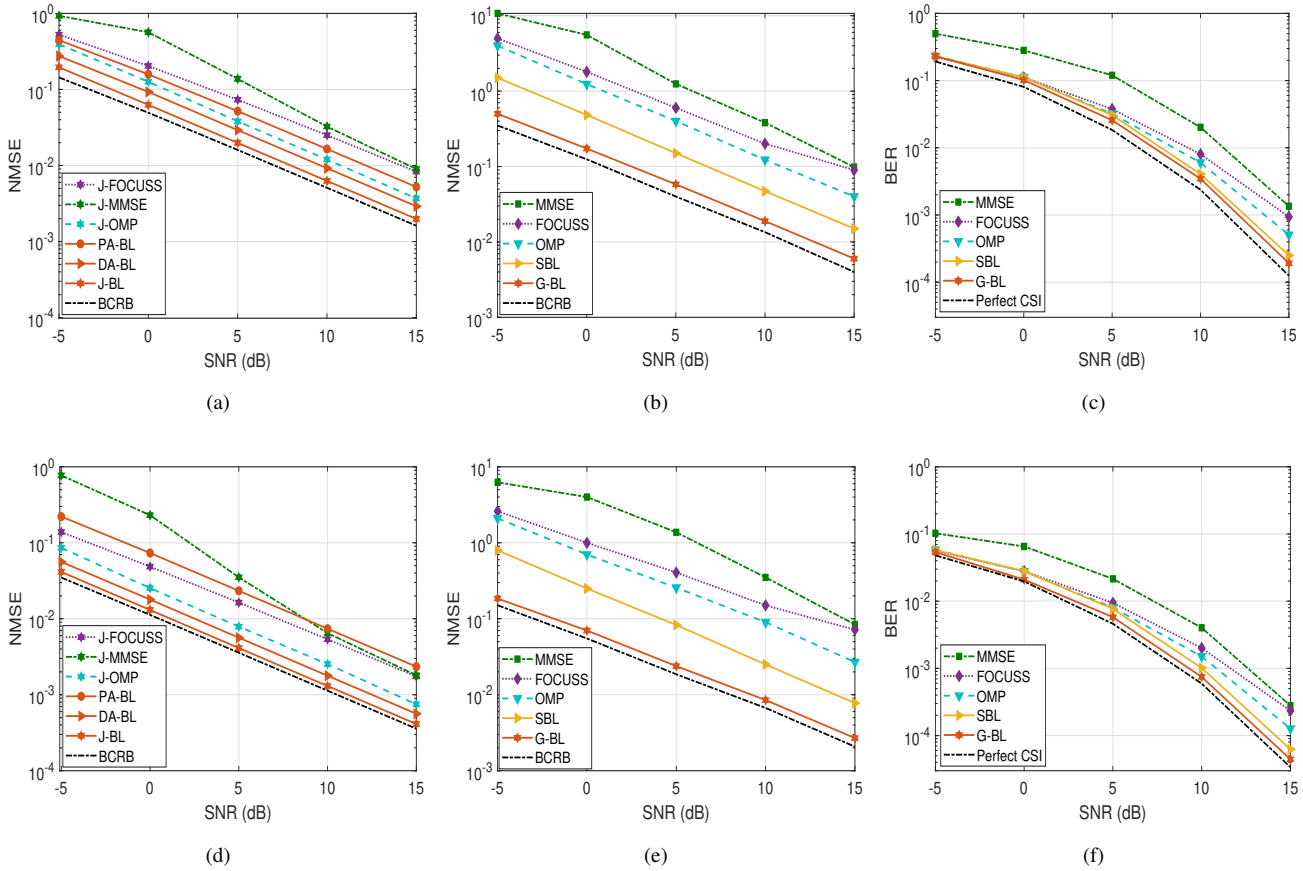

FIGURE 4: (a) NMSE versus SNR performance of RCS estimation for System-1; (b) NMSE versus SNR performance of channel estimation for System-1; (c) BER versus SNR performance for System-1; (d) NMSE versus SNR performance of RCS estimation for System-2; (e) NMSE versus SNR performance of channel estimation for System-2; (f) BER versus SNR performance for System-2.

model. Results are presented for System-1 and System-2 in Fig. 4a and Fig. 4d, respectively. Moreover, the performance of the proposed schemes is also benchmarked against the BCRB derived in (86) for the J-BL. The NMSE of the RCS matrix estimate of the radar target is defined as

$$\text{NMSE} \doteq \frac{||\widehat{\mathbf{\Gamma}}_t - \mathbf{\Gamma}_t||_F^2}{||\mathbf{\Gamma}_t||_F^2}.$$

One can observe that the J-BL algorithm results in the lowest estimation NMSE, while the PA-BL has the worst NMSE performance. This is attributed to the fact that the output sizes of the PAR, DAR and JPDR models are directly proportional to the number of pilot symbols, data symbols and the sum of pilot and data symbols, respectively, and the fact that in a typical wireless system, the number of pilot symbols is significantly smaller in comparison to the data symbols. This can also be observed from System-1, in which the output sizes of the JPDR, DAR, and PAR models are $KN_cLN_F = 5120$, $KN_c(LN_F - M_p) = 4096$ and $KN_cM_p = 1024$, respectively. An increase in the number of observation sizes naturally enhances the estimation accuracy [44], which justifies the superior NMSE performance of the JPDR in comparison to its competitors. The J-BL algorithm results in a significantly lower estimation NMSE than the competing schemes such as J-OMP, J-FOCUSS and J-MMSE. One can observe from Fig. 4a, a significant NMSE improvement of around 3 dB, 7 dB and 7.2 dB of the proposed J-BL scheme in comparison to the J-OMP, J-FOCUSS and J-MMSE, respectively. The poor performance of the OMP algorithm is due to its sensitivity both to the threshold and to the choice of the sensing matrix. Even a minor variation in the stopping parameters leads to potential structural and convergence errors. Additionally, every incorrect column selection in an iteration affects all subsequent iterations, triggering potential error propagation [38]. Furthermore, the effectiveness of FOCUSS is also limited by convergence problems and by its sensitivity to the regularization parameter [45]. Since the MMSE estimator ignores the sparsity of $\boldsymbol{\gamma}_t$, it leads to the poorest NMSE performance.

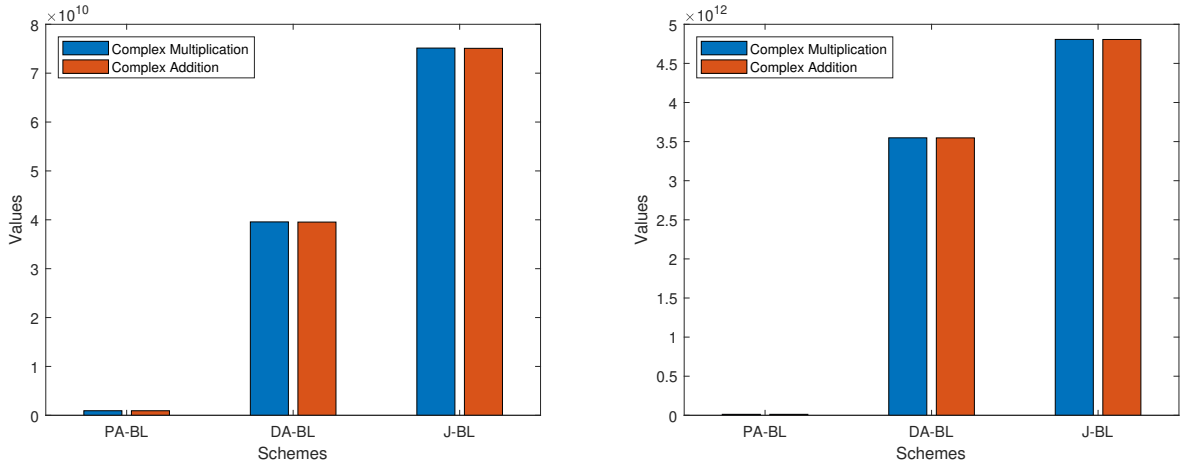

FIGURE 5: Computational Complexity of PA-BL, DA-BL and J-BL for (a) System-1; (b) System-2.

Furthermore, the performance gap between the PA-BL and DA-BL schemes increases from 2 dB in System-1, to 6 dB in System-2, as seen in Fig. 4a and Fig. 4d. This is explained by the fact that the pilot overhead for System-2 is $M_P/LN_F = 0.1$, whereas it equals 0.2 for System-1. Thus, the relative pilot length normalized by the data record size is reduced in System-2, resulting in the poor performance of the PA-BL scheme in comparison to its DA-BL counterpart. In addition, the performance of the J-BL algorithm is close to that of the BCRB, although the J-BL assumes neither the knowledge of the covariance matrix nor the support of the sparse RCS vector. This demonstrates the efficiency of the proposed scheme. Interestingly, the NMSE gap between J-BL and BCRB is lower for System-2 than for System-1. This is due to the fact that the number of observations in System-2 is $40,960$, which is increased compared to System-1 having 5120, which in turn is due to increasing the number of subcarriers K from 32 to 64 and the number of OFDM blocks L from 5 for System-1 to 20 System-2. This naturally leads to superior estimation performance.

B. Wireless channel estimation and data detection

For wireless channel estimation, we assume that the UE is equipped with $M_R = 8$ antennas and $M_{RF} = 2$ RFCs. The size of the angular grid at the receiver is $P = 10$. The number of combining vectors in $M_{CF} = 4$ combining frames is $M_{CU} = 8$. The complex path gains β_l are generated as i.i.d. samples obeying the distribution $\mathcal{CN}(0, 1)$. Moreover, the quantities ϕ_l and θ_l are randomly drawn from the interval $[0, \pi]$. The NMSE of channel estimation is defined as

$$\text{NMSE} \doteq \frac{\sum_{k=0}^{K-1} ||\widehat{\mathbf{H}}_f[k] - \mathbf{H}_f[k]||_F^2}{\sum_{k=0}^{K-1} ||\mathbf{H}_f[k]||_F^2}.$$

Fig. 4b and 4e illustrate the NMSE vs SNR of CSI estimation at the UE. The figures clearly demonstrate that the proposed G-BL yields a significantly improved performance in comparison to the SBL, OMP, and FOCUSS that also exploit the sparsity. Despite being a Bayesian learning strategy, the output of SBL suffers as it does not leverage the group sparsity inherent in $\mathbf{h}_{b,f}$. This shows clearly the benefits that can be accrued via exploiting it for sparse signal recovery in our ISAC system. Once again, the existing sparse estimation techniques such as FOCUSS and OMP lead to subpar performance, as already observed and interpreted previously for the NMSE of RCS estimation at the DFRC BS. The NMSE improvement of G-BL at the UE over the competing techniques is higher for System-2, which can once again be attributed to the overall increase in the number of pilot beams and subcarriers.

The bit error rate (BER) performance of the detection at the UE is revealed by Fig. 4c and 4f. Additionally, the BER performance is compared to a hypothetical receiver having perfect CSI. The BER associated with BL-based schemes, such as SBL and G-BL, is superior to that of the non-BL schemes, such as OMP, FOCUSS, and MMSE. This is due to the superior CSI estimation capability of the former, which is consistent with the NMSE plots of Fig. 4b and 4e. Additionally, the G-BL receiver approaches the BER of the perfect CSI-based receiver, which demonstrates its enhanced capability of CSI recovery. One can also observe the BER performance improvement of System-2, in comparison to System-1, as depicted in the Fig. 4f. This is once again a reflection of the superior NMSE performance of the System-2.

C. Computational Complexity Analysis

It is important to note that while the PAR, DAR and JPDR models may appear similar, their performance in NMSE and

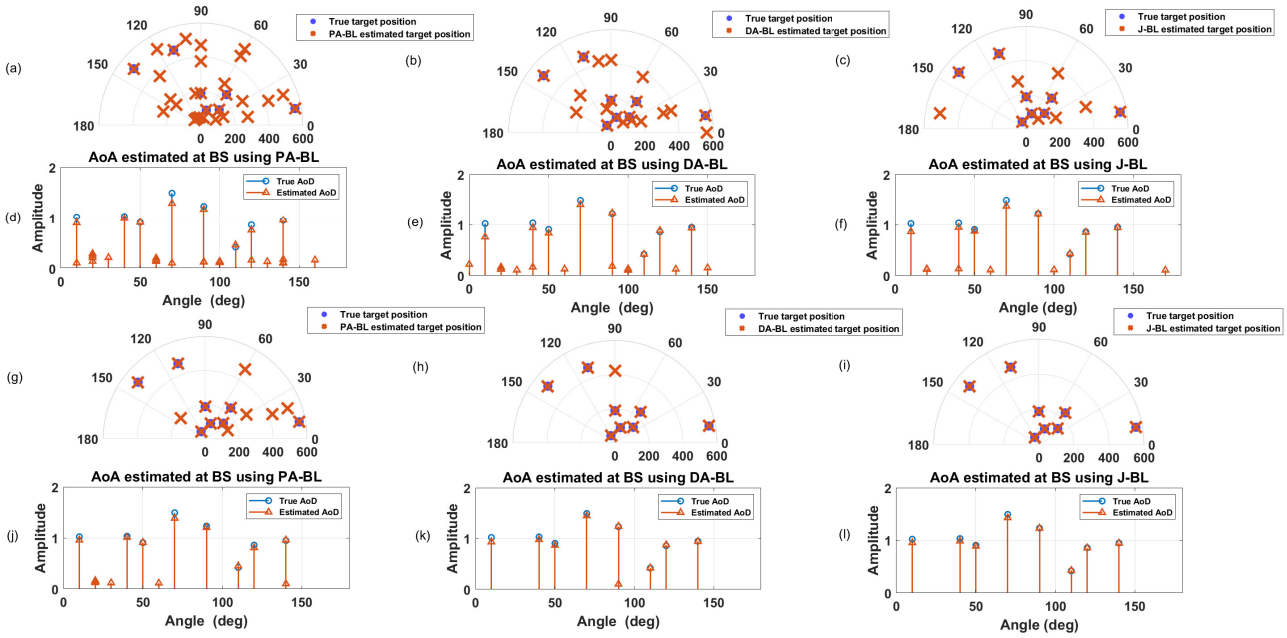

FIGURE 6: Demonstration of parameter estimation by proposed PA-BL, DA-BL and J-BL techniques at SNR= -5 dB and SNR= 5 dB with threshold $\eta = 0.1$. 5(a)-5(f) are for SNR= -5 dB and 5(g)-5(l) are for SNR= 5 dB : (a) Angle and range estimated at SNR $= -5$ dB using PA-BL (b) DA-BL (c) J-BL (d) Estimated RCS coefficient magnitudes at SNR $= -5$dB using PA-BL (e) DA-BL (f) J-BL (g) Angle and range estimated at SNR $= 5$ dB using PA-BL (h) DA-BL (i) J-BL (j) Estimated RCS coefficient magnitudes at SNR $= 5$ dB using PA-BL (k) DA-BL (l) J-BL.

computational complexities differ significantly. It can be seen that the PA-BL, DA-BL and J-BL techniques have complexities orders of $\mathcal{O}(K^3N_C^3M_P^3 + Q^3R^3)$, $\mathcal{O}(K^3N_C^3(LN_F - M_P)^3 + Q^3R^3)$ and $\mathcal{O}(K^3N_C^3L^3N_F^3 + Q^3R^3)$ per EM iteration, respectively, which arise due to the matrix inversion required to compute the *a posteriori* covariance matrix in equation (44). This difference in the computational complexities can be seen in Fig. 5a and 5b. The JPDR model can deliver superior NMSE performance compared to its PAR counterpart. However, this improvement comes at the cost of higher computational cost. Conversely, the PAR model offers lower computational complexity, but sacrifices the NMSE performance. Moreover, the performance of the DAR lies in between that of the PAR and JPDR models. Therefore, when the BS has to prioritize accuracy over complexity, the JPDR model is a suitable choice. On the other hand, in the scenario when the computational resources are limited, the BS may opt for the PAR model.

D. 2D imaging

Upon obtaining the estimate of the TD RCS matrix $\widehat{\mathbf{\Gamma}}_t$, 2D-imaging of the scattering scene can now be performed via plotting its magnitude across the angle and range bins. The presence of any target in the angle-range bin (θ_q, r) bin is reliably detected if $|\widehat{\alpha}_t(q,r)| > \eta$, where $\eta \ll 1$ is a suitably chosen threshold. Furthermore, if $\mathcal{S}$ is the set of all the (θ_q, r) bins satisfying the detection criterion, then number of targets that can be detected is given by $\widehat{L}_t = |\mathcal{S}|$. Fig. 6(a)-(i) characterize the imaging performance of proposed PA-BL, DA-BL and J-BL methods at SNR $= -5$ dB and SNR= 5 dB, with a threshold of $\eta = 0.1$, for System-1. Fig. 6(a)-(c) and Fig. 6(g)-(i) represent the angle and range estimates at SNR= -5 dB and SNR= 5 dB, respectively. Observe from Fig. 6(a)-(c), that PA-BL results in a significantly higher false positive rate, which is lower in DA-BL, with J-BL leading to the lowest rate, a trend that is consistent with their NMSE performance of RCS estimation as seen from Fig. 4a and Fig. 4d. The type-I error rate is further reduced at SNR= 5 dB, as evident from Fig. 6(g)-(l). Fig. 6(d)-(f) and Fig. 6(j)-(l) show the magnitude of the RCS coefficients evaluated at the estimated AoAs for both SNR $= -5$ dB and SNR $= 5$ dB. It is noteworthy that increasing the SNR not only improves the estimation accuracy of the RCS values for the true targets, but also reduces the false positive rate.

E. Optimal pilot power and achievable spectral efficiency

Fig. 7a illustrates the variation of the BER performance of G-BL upon varying the average pilot power ρ_c for different values of SNR= $\{0, 5, 10, 15\}$ dB. Interestingly, one can observe that the optimal pilot power, at which the minimum BER is achieved, is close to $\rho_c = 0.5$. The BER is higher for $\rho_c \leq 0.5$, since the pilot is allocated lower power, resulting in a poor channel estimate that degrades the BER performance.

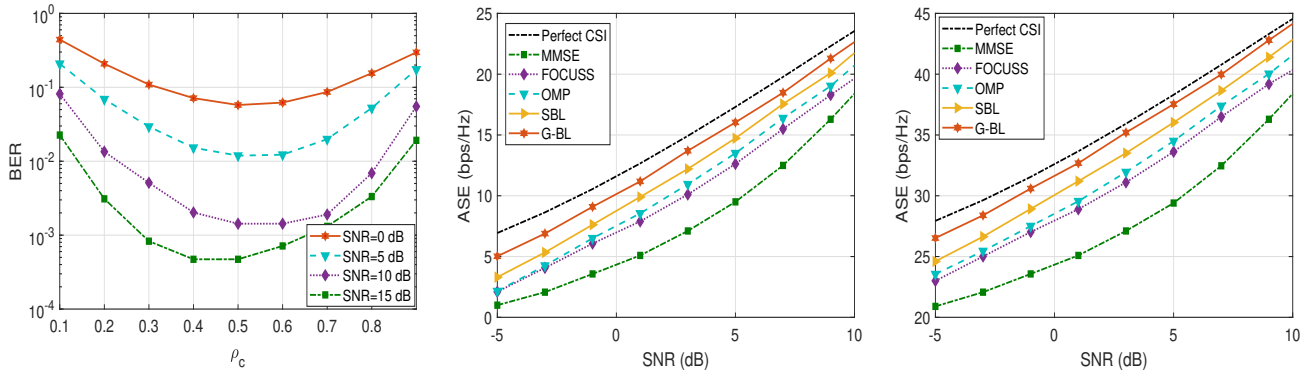

(a) (b) (c)

FIGURE 7: (a) BER versus average pilot power (ρ_c) performance; (b) Achievable spectral efficiency versus SNR for System-1; (c) Achievable spectral efficiency versus SNR for System-2.

On the other hand, for $\rho_c \geq 0.5$, while the quality of the channel estimate improves, the BER performance is once again poor, since now lower power is assigned to the data, hence resulting in a lower Euclidean distance between the constellation points. Hence, for all simulations of this paper, ρ_c is set to its optimal value, which equals to 0.5. Fig. 7b and 7c show the achievable spectral efficiency (ASE) of the G-BL and contrasted to that of SBL, OMP, FOCUSS and MMSE. The performance of a hypothetical receiver having perfect CSI and fully digital TPC and RC is also shown as a performance bound. The ASE is evaluated using the procedure outlined in [39], which can be defined as

$$\text{ASE} \doteq \frac{1}{K}\sum_{k=1}^{K}\sum_{s=1}^{N_s}\log\left(1+\frac{\text{SNR}}{N_s}\lambda_s\left(\underline{\mathbf{H}}_f[k]\right)^2\right), \quad (92)$$

where $\lambda_s\left(\underline{\mathbf{H}}_f[k]\right)$, $s=1,2,...,N_s$ represents the sth eigen value of the effective channel $\underline{\mathbf{H}}_f[k]$. The matrix $\underline{\mathbf{H}}_f[k]$ can be expressed as

$$\underline{\mathbf{H}}_f[k] = \left[\underline{\mathbf{U}}[k](:,1:N_s)\right]^H \mathbf{H}_f[k]\left[\underline{\mathbf{V}}[k](:,1:N_s)\right],$$

where $\underline{\mathbf{U}}[k](:,1:N_s)$ and $\underline{\mathbf{V}}[k](:,1:N_s)$ are the N_s dominant left and right singular vectors. The simulation parameters are set as shown in Table 4. From Fig. 7b, G-BL is seen to achieve a SE that is very close to that of the idealized hypothetical receiver having perfect CSI. It is remarkable to note that the G-BL algorithm achieves this without prior knowledge of the channel's covariance or the channel's TD support, which makes it well suited for practical deployment. The OMP and FOCUSS schemes have performance gaps of approximately 2 dB and 2.5 dB, respectively, with respect to G-BL at high SNR, confirming the superior performance of the latter in comparison to the benchmarks. Fig. 7c shows the ASE performance of System-2. It is interesting to note an ASE improvement of 22 bps/Hz, which is in line with our previous observation regarding its improved NMSE performance.

VIII. Conclusions

Bandwidth-efficient superimposed pilot-based parameter estimation scheme were conceived for mmWave MIMO-OFDM ISAC systems. Initially, the pilot-assisted radar (PAR) and data-assisted radar (DAR) models were separately developed for this mmWave MIMO-OFDM ISAC system relying on hybrid beamforming. Subsequently, these were combined into a single model to harness the power of both the known signals at the DFRC BS. Then on BL-based J-BL algorithm was developed for exploiting the sparsity of the scattering environment for enhanced radar parameter estimation. In continuation, the advanced G-BL technique was proposed for estimating the CFR at the UE in the mmWave ISAC system, which exploits the group sparsity of the joint beamspace channel across the pilot subcarriers. A framework was also developed to derive the optimal TPC, RC and pilot signal via the minimization of the total coherence of the sensing matrices. The pertinent BCRBs were developed for analytically characterizing the error covariance and MSE performance of the parameter estimation schemes designed for radar and communication. Our simulation results illustrated the efficacy of the proposed schemes over the conventional OMP and FOCUSS schemes, as well as the SBL, for radar target parameter and wireless channel estimation. Furthermore, the proposed schemes were seen to achieve an estimation performance close to the ideal BCRB, which demonstrated their efficiency.

The AP-SIP framework considered in this paper is for stationary targets. Future research may explore the proposed AP-SIP framework for mobile targets, thus incorporating the effects of Doppler shifts.

IX. Appendix

A. Optimal pilot matrix

Let us formulate the singular value decomposition (SVD) of $\mathbf{X}_{p,m}[k] = \mathbf{Q}_1\mathbf{\Sigma}\mathbf{Q}_2^H$, where $\mathbf{Q}_1$ and $\mathbf{Q}_2$ are the left and right

singular matrices of $\mathbf{X}_{p,m}[k]$, respectively. The matrix $\mathbf{\Sigma} \in \mathbb{C}^{N_{RF} \times \frac{M_P}{N_F}}$ is the singular matrix, which has the structure

$$\mathbf{\Sigma} = \left[\text{Diag}\left(\sigma_1, \sigma_2, ..., \sigma_{\frac{M_P}{N_F}} \right) \ \mathbf{0}_{\left(N_{RF} - \frac{M_P}{N_F}\right) \times \frac{M_P}{N_F}} \right]^T. \tag{93}$$

Upon employing this decomposition, the optimization problem in (77) can be recast as

$$\begin{aligned} \sigma_j^\star = \underset{\sigma_j, 1 \leq j \leq \frac{M_P}{N_F}}{\text{argmin}} \quad & \sum_{j=1}^{\frac{M_P}{N_F}} \sigma_j^4 \\ \text{s.t.} \quad & \sum_{j=1}^{\frac{M_P}{N_F}} \sigma_j^2 = \rho_c N_{RF} \frac{M_P}{N_F}. \end{aligned} \tag{94}$$

The above problem can be solved invoking the Karush-Kuhn-Tucker (KKT) conditions which yield $\sigma_j^\star = \sqrt{\rho_c N_{RF}}, \forall 1 \leq j \leq \frac{M_P}{N_F}$. The substitution of $\sigma_j^\star$ in (93) gives the desired result.

REFERENCES

[1] C. X. Wang, X. You, X. Gao, X. Zhu, Z. Li, C. Zhang, H. Wang, Y. Huang, Y. Chen, H. Haas, J. S. Thompson, E. G. Larsson, M. D. Renzo, W. Tong, P. Zhu, X. Shen, H. V. Poor, and L. Hanzo, "On the road to 6G: Visions, requirements, key technologies, and testbeds," *IEEE Communications Surveys and Tutorials*, vol. 25, no. 2, pp. 905–974, 2023.

[2] L. H. Shen, K. T. Feng, and L. Hanzo, "Five facets of 6G: Research challenges and opportunities," *ACM Comput. Surv.*, vol. 55, no. 11, feb 2023. [Online]. Available: https://doi.org/10.1145/3571072

[3] F. Boccardi, R. W. Heath, A. Lozano, T. L. Marzetta, and P. Popovski, "Five disruptive technology directions for 5G," *IEEE Communications Magazine*, vol. 52, no. 2, pp. 74–80, 2014.

[4] I. A. Hemadeh, K. Satyanarayana, M. El-Hajjar, and L. Hanzo, "Millimeter-wave communications: Physical channel models, design considerations, antenna constructions, and link-budget," *IEEE Communications Surveys and Tutorials*, vol. 20, no. 2, pp. 870–913, 2018.

[5] T. S. Rappaport, S. Sun, R. Mayzus, H. Zhao, Y. Azar, K. Wang, G. N. Wong, J. K. Schulz, M. Samimi, and F. Gutierrez, "Millimeter wave mobile communications for 5G cellular: It will work!" *IEEE Access*, vol. 1, pp. 335–349, 2013.

[6] H. Griffiths, L. Cohen, S. Watts, E. Mokole, C. Baker, M. Wicks, and S. Blunt, "Radar spectrum engineering and management: Technical and regulatory issues," *Proceedings of the IEEE*, vol. 103, no. 1, pp. 85–102, 2014.

[7] B. Paul, A. R. Chiriyath, and D. W. Bliss, "Survey of RF communications and sensing convergence research," *IEEE Access*, vol. 5, pp. 252–270, 2016.

[8] R. W. Heath, N. Gonzalez-Prelcic, S. Rangan, W. Roh, and A. M. Sayeed, "An overview of signal processing techniques for millimeter wave MIMO systems," *IEEE Journal of Selected Topics in Signal Processing*, vol. 10, no. 3, pp. 436–453, 2016.

[9] S. K. Yong and C.-C. Chong, "An overview of multigigabit wireless through millimeter wave technology: Potentials and technical challenges," *EURASIP Journal on wireless communications and networking*, vol. 2007, pp. 1–10, 2006.

[10] J. Hasch, E. Topak, R. Schnabel, T. Zwick, R. Weigel, and C. Waldschmidt, "Millimeter-wave technology for automotive radar sensors in the 77 GHz frequency band," *IEEE Transactions on Microwave theory and techniques*, vol. 60, no. 3, pp. 845–860, 2012.

[11] C. H. Doan, S. Emami, D. A. Sobel, A. M. Niknejad, and R. W. Brodersen, "Design considerations for 60 GHz CMOS radios," *IEEE Communications Magazine*, vol. 42, no. 12, pp. 132–140, 2004.

[12] Z. Pi and F. Khan, "An introduction to millimeter-wave mobile broadband systems," *IEEE Communications Magazine*, vol. 49, no. 6, pp. 101–107, 2011.

[13] M. Bică and V. Koivunen, "Generalized multicarrier radar: Models and performance," *IEEE Transactions on Signal Processing*, vol. 64, no. 17, pp. 4389–4402, 2016.

[14] K. Venugopal, A. Alkhateeb, N. G. Prelcic, and R. W. Heath, "Channel estimation for hybrid architecture-based wideband millimeter wave systems," *IEEE Journal on Selected Areas in Communications*, vol. 35, no. 9, pp. 1996–2009, 2017.

[15] J. K. Tugnait and W. Luo, "On channel estimation using superimposed training and first-order statistics," in *2003 IEEE International Conference on Acoustics, Speech, and Signal Processing, 2003. Proceedings.(ICASSP'03).*, vol. 4. IEEE, 2003, pp. IV–624.

[16] N. N. Tran, D. H. Pham, H. D. Tuan, and H. H. Nguyen, "Orthogonal affine precoding and decoding for channel estimation and source detection in MIMO frequency-selective fading channels," *IEEE Transactions on Signal Processing*, vol. 57, no. 3, pp. 1151–1162, 2008.

[17] C. Sturm and W. Wiesbeck, "Waveform design and signal processing aspects for fusion of wireless communications and radar sensing," *Proceedings of the IEEE*, vol. 99, no. 7, pp. 1236–1259, 2011.

[18] C. Shi, Y. Wang, F. Wang, S. Salous, and J. Zhou, "Joint optimization scheme for subcarrier selection and power allocation in multicarrier dual-function radar-communication system," *IEEE Systems Journal*, vol. 15, no. 1, pp. 947–958, 2020.

[19] M. Bică and V. Koivunen, "Radar waveform optimization for target parameter estimation in cooperative radar-communications systems," *IEEE Transactions on Aerospace and Electronic Systems*, vol. 55, no. 5, pp. 2314–2326, 2018.

[20] X. Hu, C. Masouros, F. Liu, and R. Nissel, "MIMO-OFDM dual-functional radar-communication systems: Low-PAPR waveform design," *arXiv preprint arXiv:2109.13148*, 2021.

[21] J. An, H. Li, D. W. K. Ng, and C. Yuen, "Fundamental detection probability vs. achievable rate tradeoff in integrated sensing and communication systems," *IEEE Transactions on Wireless Communications*, pp. 1–1, 2023.

[22] M. F. Keskin, H. Wymeersch, and V. Koivunen, "MIMO-OFDM joint radar-communications: Is ICI friend or foe?" *IEEE Journal of Selected Topics in Signal Processing*, vol. 15, no. 6, pp. 1393–1408, 2021.

[23] P. Kumari, J. Choi, N. González-Prelcic, and R. W. Heath, "IEEE 802.11 ad-based radar: An approach to joint vehicular communication-radar system," *IEEE Transactions on Vehicular Technology*, vol. 67, no. 4, pp. 3012–3027, 2017.

[24] S. H. Dokhanchi, B. S. Mysore, K. V. Mishra, and B. Ottersten, "A mmWave automotive joint radar-communications system," *IEEE Transactions on Aerospace and Electronic Systems*, vol. 55, no. 3, pp. 1241–1260, 2019.

[25] F. Liu, C. Masouros, A. P. Petropulu, H. Griffiths, and L. Hanzo, "Joint radar and communication design: Applications, state-of-the-art, and the road ahead," *IEEE Transactions on Communications*, vol. 68, no. 6, pp. 3834–3862, 2020.

[26] S. D. Liyanaarachchi, C. B. Barneto, T. Riihonen, M. Heino, and M. Valkama, "Joint multi-user communication and MIMO radar through full-duplex hybrid beamforming," in *2021 1st IEEE International Online Symposium on Joint Communications and Sensing (JC&S)*, 2021, pp. 1–5.

[27] A. M. Elbir, K. V. Mishra, A. Abdallah, A. Celik, and A. M. Eltawil, "Spatial path index modulation in mmWave/THz-band integrated sensing and communications," *arXiv preprint arXiv:2303.12328*, 2023.

[28] S. D. Liyanaarachchi, C. B. Barneto, T. Riihonen, M. Heino, and M. Valkama, "Range–angle processing for target detection in joint MIMO-OFDM communications and sensing," in *2021 IEEE 22nd International Workshop on Signal Processing Advances in Wireless Communications (SPAWC)*. IEEE, 2021, pp. 486–490.

[29] M. L. Rahman, J. A. Zhang, X. Huang, Y. J. Guo, and R. W. Heath, "Framework for a perceptive mobile network using joint communication and radar sensing," *IEEE Transactions on Aerospace and Electronic Systems*, vol. 56, no. 3, pp. 1926–1941, 2019.

[30] M. L. Rahman, J. A. Zhang, X. Huang, Y. J. Guo, and Z. Lu, "Joint communication and radar sensing in 5G mobile network by compressive sensing," *IET Communications*, vol. 14, no. 22, pp. 3977–3988, 2020.

[31] Z. Gao, Z. Wan, D. Zheng, S. Tan, C. Masouros, D. W. K. Ng, and S. Chen, "Integrated sensing and communication with mmWave massive MIMO: A compressed sampling perspective," *IEEE Transactions on Wireless Communications*, vol. 22, no. 3, pp. 1745–1762, 2023.

[32] D. Bao, G. Qin, and Y.-Y. Dong, "A superimposed pilot-based integrated radar and communication system," *IEEE Access*, vol. 8, pp. 11 520–11 533, 2020.
[33] I. Gorodnitsky and B. Rao, "Sparse signal reconstruction from limited data using focuss: a re-weighted minimum norm algorithm," *IEEE Transactions on Signal Processing*, vol. 45, no. 3, pp. 600–616, 1997.
[34] T. T. Cai and L. Wang, "Orthogonal matching pursuit for sparse signal recovery with noise," *IEEE Transactions on Information Theory*, vol. 57, no. 7, pp. 4680–4688, 2011.
[35] G. Li, Z. Zhu, D. Yang, L. Chang, and H. Bai, "On projection matrix optimization for compressive sensing systems," *IEEE Transactions on Signal Processing*, vol. 61, no. 11, pp. 2887–2898, 2013.
[36] J. A. Zhang, F. Liu, C. Masouros, R. W. Heath, Z. Feng, L. Zheng, and A. Petropulu, "An overview of signal processing techniques for joint communication and radar sensing," *IEEE Journal of Selected Topics in Signal Processing*, vol. 15, no. 6, pp. 1295–1315, 2021.
[37] S. Liu and O. Trenkler, "Hadamard, Khatri-Rao, Kronecker and other matrix products," *International Journal of Information and Systems Sciences*, vol. 4, 01 2008.
[38] D. P. Wipf and B. D. Rao, "Sparse Bayesian learning for basis selection," *IEEE Transactions on Signal processing*, vol. 52, no. 8, pp. 2153–2164, 2004.
[39] J. Rodríguez-Fernández, N. González-Prelcic, K. Venugopal, and R. W. Heath, "Frequency-domain compressive channel estimation for frequency-selective hybrid millimeter wave MIMO systems," *IEEE Transactions on Wireless Communications*, vol. 17, no. 5, pp. 2946–2960, 2018.
[40] S. Srivastava, A. Mishra, A. Rajoriya, A. K. Jagannatham, and G. Ascheid, "Quasi-static and time-selective channel estimation for block-sparse millimeter wave hybrid MIMO systems: Sparse Bayesian learning (SBL) based approaches," *IEEE Transactions on Signal Processing*, vol. 67, no. 5, pp. 1251–1266, 2019.
[41] J. Lee, G.-T. Gil, and Y. H. Lee, "Channel estimation via orthogonal matching pursuit for hybrid MIMO systems in millimeter wave communications," *IEEE Transactions on Communications*, vol. 64, no. 6, pp. 2370–2386, 2016.
[42] P. Singh, S. Srivastava, A. K. Jagannatham, and L. Hanzo, "Second-order statistics-based semi-blind techniques for channel estimation in millimeter-wave MIMO analog and hybrid beamforming," *IEEE Transactions on Communications*, vol. 68, no. 11, pp. 6886–6901, 2020.
[43] H. L. V. Trees and K. L. Bell, *Bayesian Bounds for Parameter Estimation and Nonlinear Filtering/Tracking*. Wiley-IEEE Press, 2007.
[44] S. M. Kay, *Fundamentals of statistical signal processing: estimation theory*. USA: Prentice-Hall, Inc., 1993.
[45] I. Gorodnitsky and B. Rao, "Sparse signal reconstruction from limited data using focuss: a re-weighted minimum norm algorithm," *IEEE Transactions on Signal Processing*, vol. 45, no. 3, pp. 600–616, 1997.

AWADHESH GUPTA (Graduate Student Member, IEEE) received the B.Tech. degree in Electronics and Communication Engineering from the Gautam Buddh Technical University, Uttar Pradesh, India, in 2012, and the M.Tech. degree in Communication System Engineering from the Indian Institute of Technology Patna, Patna, India in 2015. He is currently working toward the Ph.D. degree with the Department of Electrical Engineering, Indian Institute of Technology Kanpur, Kanpur, India. From August 2015 to December 2017, he was employed as an assistant professor with SRMU, Lucknow. From January 2018 to December 2020, he was employed as an assistant professor with MITS, Gwalior under TEQIP-III project of National Project Implementation Unit (NPIU). His research interests include signal processing and optimization techniques for 5G and beyond wireless systems, Integrated Sensing and Communication (ISAC), Orthogonal Time-Frequency Space (OTFS), mmWave communication and ambient backscatter communication (AmBC).

MEESAM JAFRI (Member, IEEE) received the B.E. degree in Electronics and Communication Engineering from Jamia Millia Islamia, New Delhi, India, in 2016 and the M.Tech. degree in Communication and Information Technology from National Institute of Technology Srinagar, India, in 2018. He is currently pursuing the Ph.D. degree with the Department of Electrical Engineering, Indian Institute of Technology Kanpur, Kanpur, India. His research interests include coordinated beamforming in 5G Wireless Systems, mmWave Communication, Orthogonal Time-Frequency Space (OTFS), Radar Signal Processing, Joint Radar and Communication (RadCom). He was awarded Qualcomm Innovation Fellowship (QIF) in year 2022 from Qualcomm.

SURAJ SRIVASTAVA (Member, IEEE) received the M.Tech. degree in Electronics and Communication Engineering from Indian Institute of Technology Roorkee, India, in 2012, and Ph.D. degree in Electrical Engineering from Indian Institute of Technology Kanpur, India, in 2022. From July 2012 to November 2013, he was employed as a Staff-I systems design engineer with Broadcom Research India Pvt. Ltd., Bangalore, and from November 2013 to December 2015, he was employed as a lead engineer with Samsung Research India, Bangalore where he worked on developing layer-2 of the 3G UMTS/WCDMA/HSDPA modem. He worked as a senior lead engineer in Qulacomm India Pvt. Ltd., Bangalore, from October 2022 to November 2023. His research interests include applications of Sparse Signal Processing in 5G Wireless Systems, mmWave and Tera-Hertz Communication, Orthogonal Time-Frequency Space (OTFS), Joint Radar and Communication (RadCom), Optimization and Machine Learning. He was awarded Qualcomm Innovation Fellowship (QIF) in year 2018 and 2022 from Qualcomm. He was also awarded Outstanding Ph.D. Thesis and Outstanding Teaching Assistant awards from IIT Kanpur. He is currently an Assistant Professor at the Department of Electrical Engineering, Indian Institute of Technology Jodhpur.

ADITYA K. JAGANNATHAM (Senior Member, IEEE) received the bachelor's degree from the Indian Institute of Technology, Bombay, and the M.S. and Ph.D. degrees from the University of California at San Diego, San Diego, CA, USA. From April 2007 to May 2009, he was employed as a Senior Wireless Systems Engineer with Qualcomm Inc., San Diego, where he was a part of the Qualcomm CDMA Technologies (QCT) Division. He is currently a Professor with the Department of Electrical Engineering, IIT Kanpur, where he also holds the Arun Kumar Chair Professorship. His research interests include next generation wireless cellular and WiFi networks, with a special emphasis on various 5G technologies such as massive MIMO, mmWave MIMO, FBMC, NOMA, as well as emerging 6G technologies such as OTFS, IRS, THz systems and VLC. He has been twice awarded the P. K. Kelkar Young Faculty Research Fellowship for excellence in research, received multiple Qualcomm Innovation Fellowships (QIF 2018, 2022), the IIT Kanpur Excellence in Teaching Award, the CAL(IT)2 Fellowship at the University of California at San Diego, the Upendra Patel Achievement Award at Qualcomm San Diego and the Qualcomm 6G UR India gift.

LAJOS HANZO (FIEEE'04) received Honorary Doctorates from the Technical University of Budapest (2009) and Edinburgh University (2015). He is a Foreign Member of the Hungarian Science-Academy, Fellow of the Royal Academy of Engineering (FREng), of the IET, of EURASIP and holds the IEEE Eric Sumner Technical Field Award. For further details please see http://www-mobile.ecs.soton.ac.uk/, https://en.wikipedia.org/wiki/Lajos_Hanzo.